FINAL REPORT

CONTRACT NONR 4548 (00)

HUGHES

HUGHES AIRCRAFT COMPANY

HIGH POWERED DIFFRACTION LIMITED RAMAN LASER

15 APRIL 1965 through 14 APRIL 1966

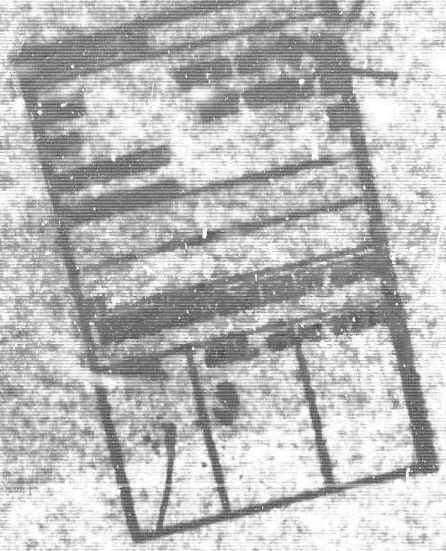

HUGHES RESEARCH LABORATORIES
Malibu, California

a division of hughes aircraft company

HIGH POWERED DIFFRACTION LIMITED RAMAN LASER

F. J. McClung, D. H. Close,
R. W. Hellwarth, and W. G. Wagner

Final Report
15 May 1965 through 14 April 1966

Contract Nonr 4849 (00)
ARPA Order No. 306

This research is part of Project DEFENDER under the joint sponsorship of the Advanced Research Projects Agency, the Office of Naval Research and the Department of Defense.

TABLE OF CONTENTS

ABSTRACT

Problems associated with the realization of a high energy, highly coherent Raman laser have been investigated. Since the discovery that the self-focusing of pump radiation and scattered radiation is present in most laboratory Raman lasers and tends to spoil the coherence of the output, the nature and mechanisms of this self-trapping have been the primary objects of study in order that it might be prevented. Time resolved photographic studies have been made which show that the small filaments of self-trapped light in the pump beam persist for only a small fraction of the beam pulse duration and are sufficiently intense to resolve the apparent discrepancy between the average intensity and observed Raman gains. Time integrated photographic studies and photometric studies showed that only purely linearly polarized light preserves its polarization after self-trapping in CS_2 and nitrobenzene. Attempts to compare measured nonlinear indices for both circular and linear polarizations with those calculated for various mechanisms were frustrated by this instability in the propagation of circularly polarized light. The instability was explained qualitatively and indicates that electrostriction is not a dominant mechanism. A classical statistical mechanical calculation of the nonlinear index of a liquid (with no macroscopic density changes) showed that the local redistribution of molecules is generally important. This effect will cause perfectly symmetric molecules to have a significant nonlinear index. It is therefore concluded that it is very unlikely that any room temperature liquid will perform as a high energy Raman laser material without beam deterioration due to self-focusing.

I. INTRODUCTION

The growth of our understanding of stimulated Raman scattering (SRS) can be characterized as a series of discoveries, preceded and followed by periods of wide divergence of theory and experiments. It could be said that our progress has been one of discovering one problem after another and slowly resolving these problems by discovery of new effects. We list here some of the problems which have plagued the development of SRS; some of them have not been resolved within the period covered by this report.

The first problem to attract attention concerned the incorrect emission angles of the anti-Stokes lines; the second problem involved the large spectral broadening due to multimode pumping, and the third concerned the large amount of anti-Stokes power and backward-radiated Stokes and anti-Stokes light. Excessively high gain and the abrupt threshold of SRS were key difficulties throughout the investigation.

In this report we show that some of these anomalies (such as the anomalous gain) can be understood to be a result of light-trapping, as we had previously predicted.[1] The presence of large amounts of anti-Stokes power, forward-to-backward Stokes ratio, and wrong cone angles, however, remain poorly understood. More puzzling in some respects is the behavior of SRS in some gases when the data "suggest" that beam-trapping may be taking place; this would certainly be surprising if it were true. From our theoretical studies, we also conclude that any liquid, even of symmetric molecules, will be expected to trap when the total power in the material (Raman or laser pump) is in excess of 10^6 to 10^7 W. However, the use of gases may permit us to handle much more power. In this report we review our work on SRS and the beam-trapping effects which have now become almost indistinguishable from SRS, although there are clearly two different effects. The discussion will be organized with the experiment and theory separate, although the two could not be and were not separated at the time.

II. MODE SELECTION

At the beginning of this contract, considerable emphasis was placed upon the fact that almost all of the theories of SRS had run into severe conflict with experiments. One of the main reasons for this sudden divergence of experiment and theory was the possibility of experiments using single mode GP lasers to study the nonlinear effects, as described in Appendix I. All of the early nonlinear work had been done with multimode lasers and the mode structure of the laser had been shown, by us and others, to cause a considerable spectral broadening of the anti-Stokes radiation. There was a large anomaly, not generally recognized, in the Raman gain; the first explanation used the multimode arguments that had been used before in a different context. The multimode theory, of course, has been shown to be correct as far as it goes, but our single mode experience showed that the theory did not explain the magnitude of the anomaly in the Raman gain, as is shown in Appendix II and elsewhere.[2]

This early work left the gain anomaly unresolved. Fortunately, the new idea of light trapping proved powerful enough to provide a resolution[3-5]; many of the features of SRS are determined by light-trapping effects, and the study of SRS has turned almost completely into the study of light-trapping.

III. STUDIES OF BEAM TRAPPING

Self-focusing and trapping phenomena in high power electromagnetic beams were foreseen by Askan'yan,[3] Talanov,[4] and Chiao, et al.[5] We later suggested[1] that this mechanism could explain some of the anomalies observed in SRS, especially the low thresholds, and the effect has since been observed in many liquids.[6-10] We discuss our experimental investigations of beam trapping in liquids, describing (1) the time-integrated photographic observations of filaments in nitrobenzene and carbon disulfide, (2) the time-resolved photographic studies of beam trapping in nitrobenzene, and (3) the polarization effects observed in beam trapping in several liquids. This report on our experimental work is followed by a discussion of how well the phenomenon of beam trapping explains the observed anomalies in SRS.

A. Time-Integrated Photographic Observations of Filaments

The experimental apparatus used for these investigations is shown schematically in Figs. 1 and 2. Figure 1 shows the mode-controlled giant pulse ruby laser system which was discussed in detail in Appendix I. Figure 2, with the STL image converter camera replaced by an ordinary camera and the 0.5 mm slit removed, shows the arrangement we used for observing filaments. In this arrangement the beam from the giant pulse laser is first accurately defined by passage through a 1.5 mm diameter aperture; it then travels through a 10 cm long sample cell where SRS occurs, and finally goes through the following optical system, along with the stimulated Raman emission.

The optical system produces dispersed, magnified images of the exit end of the sample cell on the film plane of the camera. Photographic recording of these images allows study of the size, number, contrast, etc., of filaments at the laser and at the first, second, and (for CS_2) third order Stokes wavelengths. The wavelength dispersion is accomplished by imaging the end of the sample cell through a small, high speed, diffraction grating spectrograph. The end of the cell is imaged in the entrance aperture of the spectrograph; the dispersion of the latter separates the images for the various wavelengths in the exit plane. The camera then images the exit plane of the spectrograph onto its film plane. The over-all magnification of the final image at the film plane is the product of the magnifications of the first two lenses — that through the spectrograph and that of the camera — and was typically eight times in our experiments. The resolution obtained was about 10 μ when I-N photographic plates were used, and considerably worse for infrared Polaroid film. The resolution, of course, directly determines the minimum filament size which can be inferred

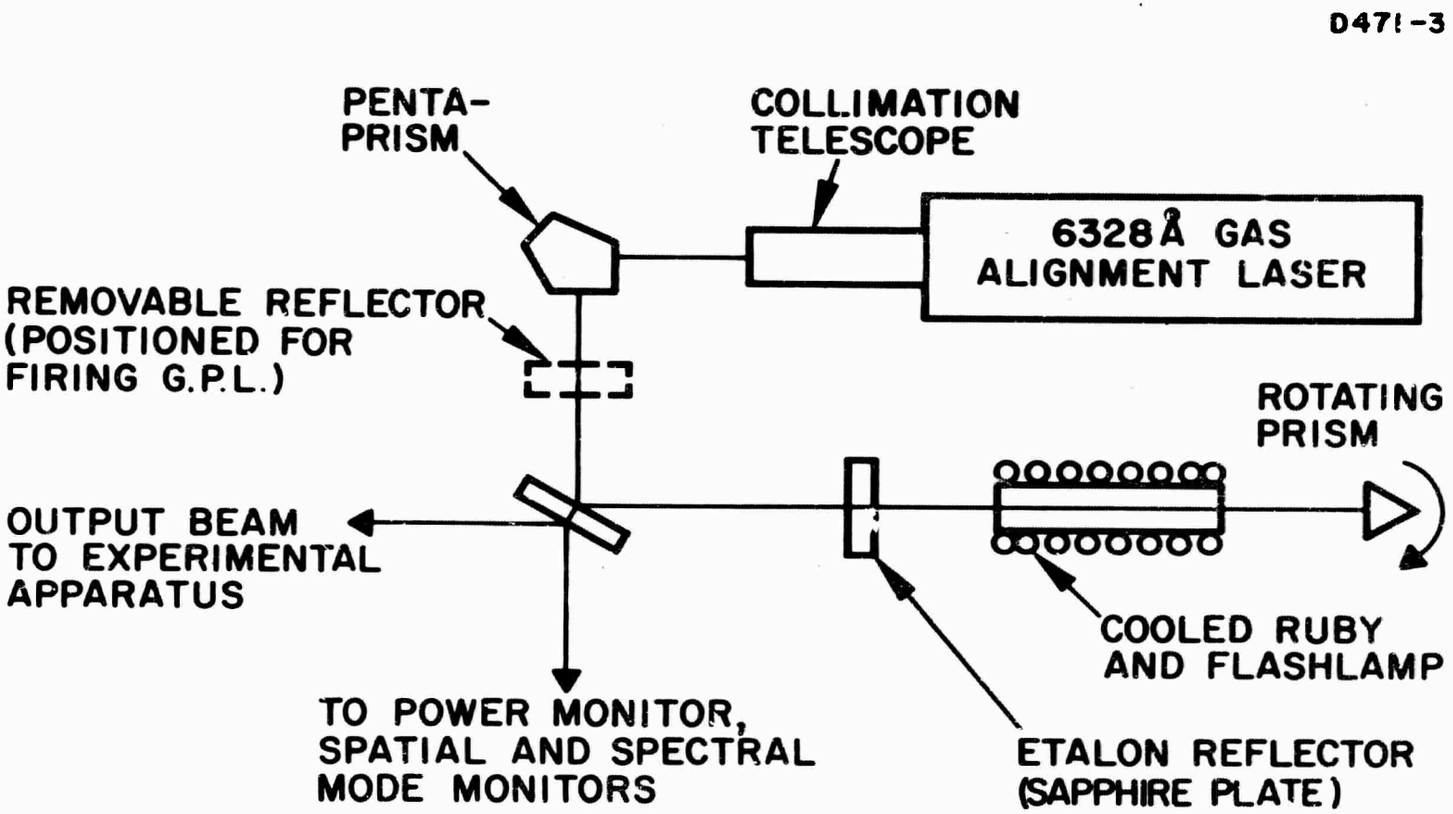

Fig. 1. Schematic diagram of the giant pulse laser system.

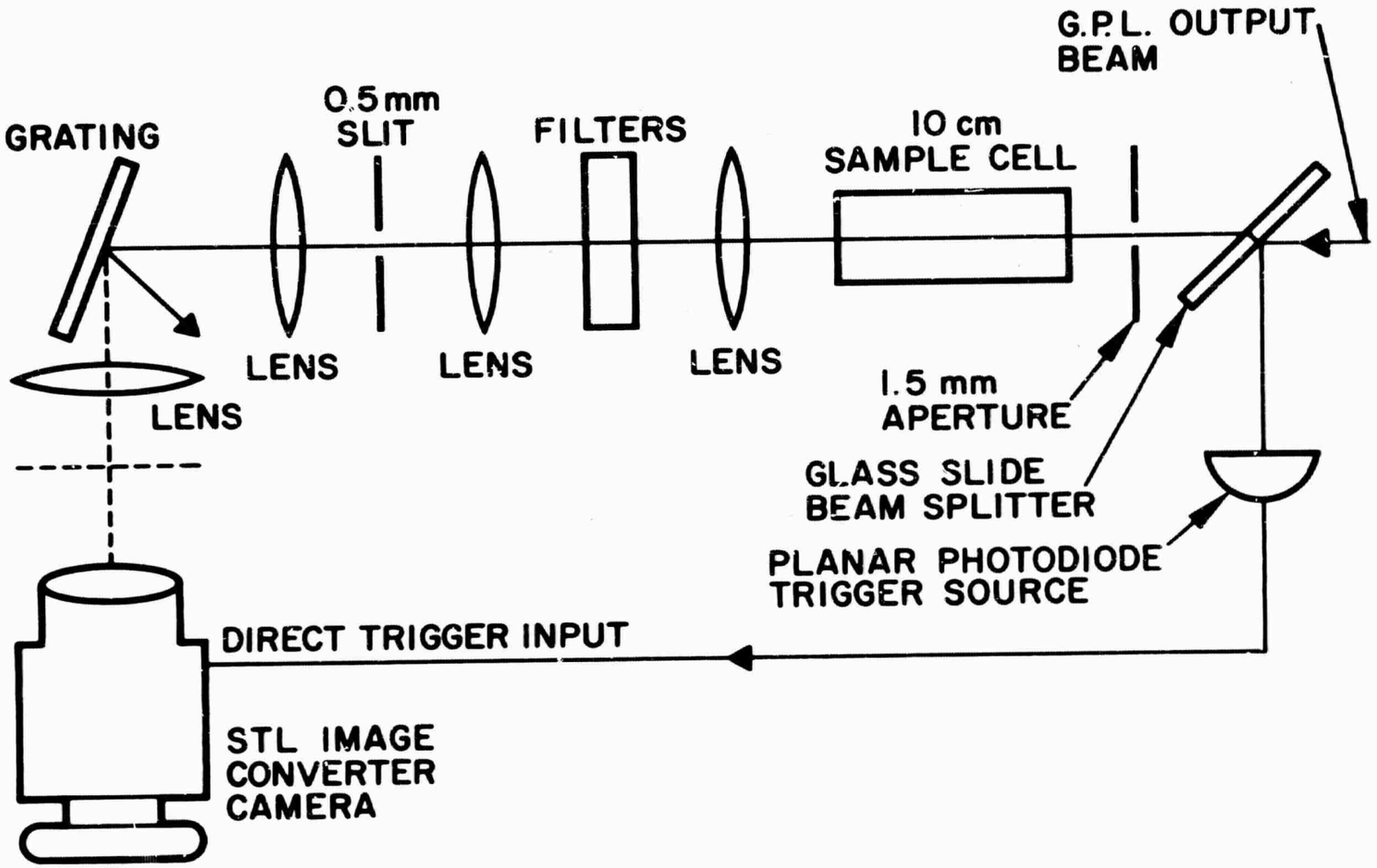

Fig. 2. Schematic diagram of the apparatus used for observing laser and Stokes filaments.

from these observations. Since only infrared Polaroid film was used in the experiments with CS_2 we do not have definitive data for that material, and will proceed to discuss the more complete observations on nitrobenzene. There is no indication of any gross difference for CS_2.

The observations of nitrobenzene filaments were made at and somewhat above SRS threshold. Typically about 10% of the laser pump beam was observed to be trapped into small filaments about 30 to 50 μ in diameter. Several filaments (5 to 10) were usually observed for a single firing of the GPL and these were of roughly equal intensity. The integrated intensity of these laser filaments was only about two to three times that of the inhomogeneous background, thus making observation of them somewhat difficult. Radiation at the first and higher order Stokes wavelengths occurred only in filaments which were usually smaller than the laser filaments. Sizes of the Stokes filaments ranged from the resolution limit, i.e., about 10 μ, up to about 30 μ in diameter. The correlation between the laser and Stokes filaments was very good, indicating that SRS was indeed occurring in the trapped laser filaments and that the Stokes radiation thus produced was also trapped in the same filamentary region. Occasionally, a Stokes filament was observed without a corresponding laser filament. This can be attributed to saturation of the laser pump radiation in that filament, with almost total conversion to Stokes radiation.

The number of laser and Stokes filaments is observed to increase uniformly with increasing pump power above threshold. The power in a single filament, however, appears to be nearly a constant.

B. Time-Resolved Photographic Studies of Filaments

The phenomenon of beam trapping can explain the anomalously low thresholds for SRS if the intensity in the trapped filament is sufficiently higher than the background intensity. As noted above, we observed a time-integrated enhancement of intensity of only two to three times in the filaments, whereas approximately a factor of 100 is needed to explain the discrepancy with theory.[1] The absence of such large enhancements in the above data can be explained if a typical filament is present for a time short compared to the total pump pulse length. Since the latter is typically 50 nsec, the filament duration should be only one or a few nanoseconds to explain the observed thresholds. In order to check this hypothesis, we undertook an investigation of the time-resolved laser and Stokes emission.

The apparatus for these experiments, shown schematically in Fig. 2, is the same as that for the time-integrated observations described above except for the STL image converter camera and a 0.5 mm

slit at the entrance aperture of the spectrograph. In order to get maximum time resolution, the fastest streak mode of operation of the STL camera was used. This was a 50 nsec sweep and resulted in a time resolution of about 1 nsec. In some experiments the 0.5 mm slit was omitted, so that a smear photograph was obtained instead of a streak photograph.

The short streak duration and the resulting high writing rate led to several experimental difficulties which limited the amount and qualify of the data. The experiments required operation of the STL camera at the limits of its capabilities. For example, some compromise had to be made between adequate exposure and overloading the electron optics in the STL camera. Two difficulties arising from this were rather poor resolution compared with that of the static photographs, and some ambiguity in interpretation of the observed data, i.e., in the decision as to whether some feature was real or caused by distortion of the electron optics. By taking some data at very low exposures and using the static photographs as a guide, we feel we have generally been able to make good interpretations of the observed data. Another major difficulty arising from the short streak duration was in proper triggering of the STL camera. The usual trigger circuits were found to be too slow, and various other triggering schemes were used. The most useful is that shown in Fig. 2, where the output of a planar ("bomb") photodiode, driven very hard by part of the GPL output, is applied directly to trigger the camera. With this arrangement we were usually able to observe the significant parts of the laser pump pulse.

Our time-resolved observations were on the laser and first Stokes radiation from nitrobenzene. As in the above observations, the laser beam was linearly polarized. The laser filaments appeared at different times lasting typically from 3 to 6 nsec. The first Stokes filaments were observed to persist for a shorter time of about 1 to 3 nsec. The peak intensity of the laser filaments relative to the background intensity could not be accurately determined because of the small contrast range inherent in the experiments, but was at least one order of magnitude higher. Comparison of the laser and Stokes filament durations and the laser pulse duration indicates that these observations explain the threshold discrepancy at least to within a factor of two.

In the time-resolved photographs we have again occasionally observed Stokes filaments without corresponding laser filaments, and very bright laser filaments with no evident associated Stokes emission. In addition, there appears to be some spatial "wandering" of the observed filaments that is not a result of distortion in the electron optics. Although these issues are not definitely settled, we feel the effects are probably due to saturation of the laser pump and the short time scale dynamics of filament formation.

C. Polarization Effects in Beam Trapping

The physical mechanism which has usually been accepted as responsible for beam trapping in liquids is molecular reorientation in the strong optical fields; this is generally termed the ac Kerr effect. Comparisons of the Kerr constants with observed thresholds in liquids which readily exhibit SRS have been usually favorable.[7-9] We have attempted to verify this molecular reorientation hypothesis by observing the filaments induced by pump light which is linearly or circularly polarized, and by seeing whether the observed thresholds for these two cases behave according to the theory of reorientation. We have made photographic and photometric studies of the polarization dependence of beam trapping in several liquids. We have found an instability in the nonlinear propagation of circularly polarized light which has made interpretation of the threshold measurements difficult. However, the origin of this instability and its consequences are interesting. A paper, "The Self-Focusing of Light of Different Polarizations," which discusses these results and which will be published in the Fourth Quantum Electronics Conference Proceedings, is reproduced here as Appendix III.

1. Photographic Techniques

The apparatus for the photographic experiments is shown schematically in Fig. 3, and is the same as that used for the static photographic studies, except that a quarter-wave plate to fix the polarization of the laser pump beam and a Fresnel rhomb and Wollaston prism to analyze the polarization of the radiation exiting from the sample cell have been added. The camera thus records dispersed images of the cell end, with polarization information at each wavelength. By setting the Wollaston prism properly, the analyzer system gives either the components of the radiation in two orthogonal linear polarizations or the components in the right and left circular polarizations.

Photographic observations were made on nitrobenzene and CS_2. If the imput beam was linearly polarized, the laser background, laser filaments, and Stokes filaments were all like-polarized to within one part in 10^3, the limit of our instrumentation. However, if the input beam was circularly polarized, each Stokes order for nitrobenzene contained equal amounts of both circular polarizations over the entire range of observation of about three orders of magnitude in the total first Stokes intensity. Furthermore, the right and left circularly polarized images at any one Stokes frequency were identical in every detail of intensity and pattern. The laser background appeared entirely in the input polarization, while the laser filaments appeared in both circular polarizations. The laser filaments also seemed to be equally intense and otherwise identical in both circular polarizations, although this was difficult to ascertain with the laser back-

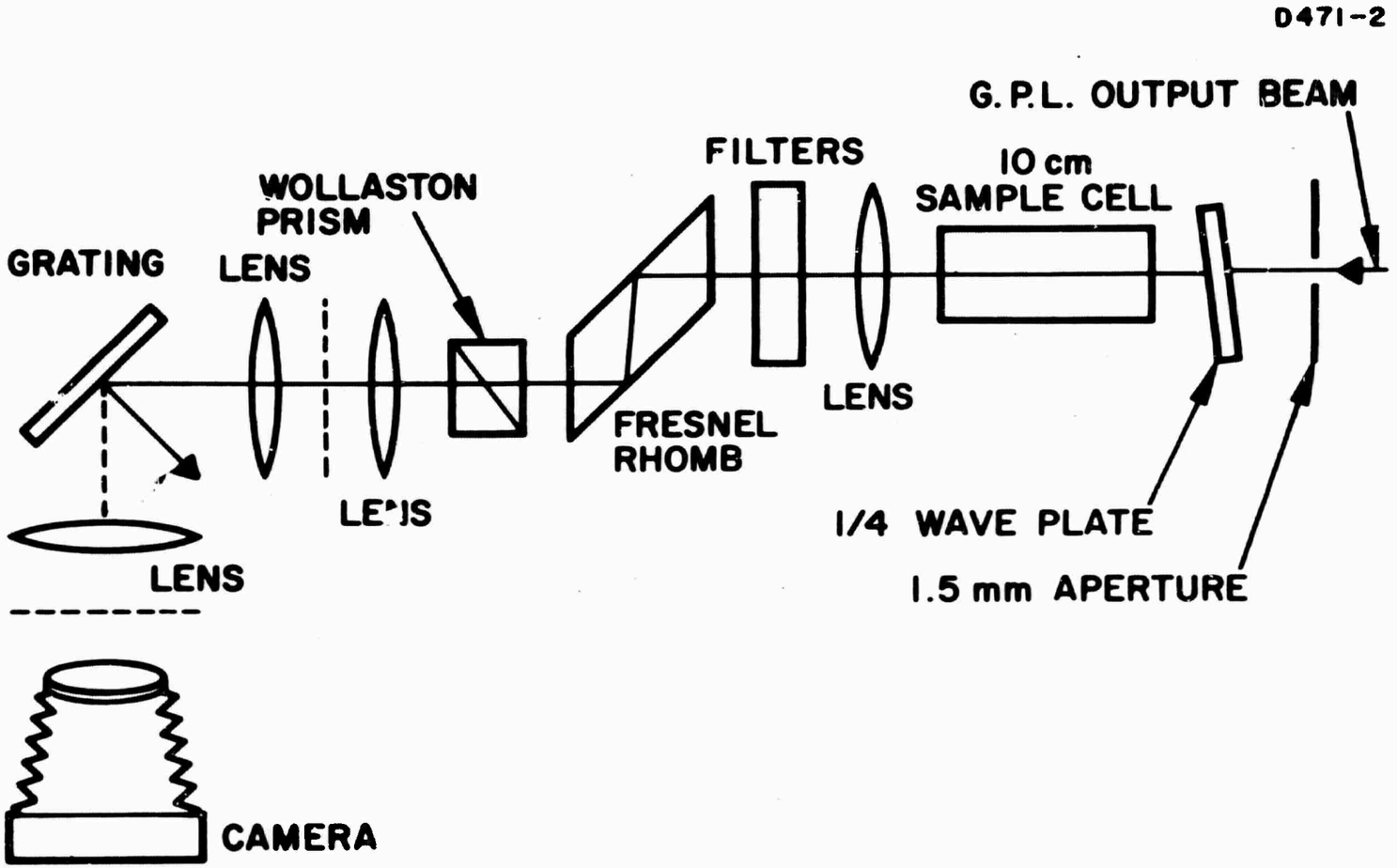

Fig. 3. Schematic diagram of the apparatus used for studying polarization effects in beam trapping.

ground appearing in the one circular polarization. When the Wollaston prism was rotated to test for orthogonal linearly polarized components with the same (circular) input polarization, the nitrobenzene Stokes filament patterns for the two linear polarizations at one frequency did differ in detail, with variations in intensity between corresponding filaments and many cases of unpaired filaments in one or the other of the polarizations. As expected, the laser background appeared equally strong in both linear polarizations, making analysis of the laser filaments difficult. The total Stokes intensity was about equal in each linear polarization at one frequency. These observations led to the interpretation that the circular input beam produces filaments in nitrobenzene which are linearly polarized, with a random direction of polarization which varies from filament to filament. The theoretical basis for these observations is discussed below.

Similar experiments with circularly polarized pump light in CS_2 showed some slightly different results. There was incomplete depolarization, with about a third of the filament energy appearing in the opposite circular polarization to that of the laser and first Stokes filaments. The partition of energy was more nearly equal in the second Stokes output and became essentially equal in the third Stokes output. This can be taken as evidence that the various Stokes orders are iteratively generated, i.e., that the laser produces the first Stokes, which in turn produces the second Stokes, etc.

Since a wide range of Stokes intensity could not be covered in the photographic observations, estimates of the relative thresholds for circular and linear input polarizations are not very accurate. By counting the number of observed Stokes filaments as a function of laser power, we found an approximate ratio of circular threshold to linear threshold of about 3.8 for nitrobenzene and 2.5 for CS_2, which can be compared with the theoretical value of 4 for the ac Kerr effect and with the more accurate photometric results below.

2. Photometric Techniques

For the photometric measurements, the unfocused beam of a giant pulse ruby laser was first passed through crossed Glan polarizers which served as a variable attenuator and supplied a purely linearly polarized output beam. The unfocused beam then passed through a quarter-wave plate and a 10 cm cell containing the liquid in which self-trapping was to be studied. A portion of the output beam from this cell was split off and monitored by silicon photodiodes for Stokes energy content after passing through a Corning 5-56 filter, two Wratten 89B filters, and appropriate attenuators. When the liquid cell was removed, the laser produced no signal at the photodetector, thus assuring that only Stokes light was being measured.

Typical results for the Stokes output powers plotted as a function of either linearly or circularly polarized inputs are given for benzene, nitrobenzene, and CS_2 in Fig. 4. From such data the trapping threshold ratios(circular to linear) for various liquids are given in Table I of Appendix III. These ratios are seen to be consistently well below the value 4 expected if circularly polarized light would produce circularly polarized filaments via the ac Kerr effect.

The depolarization of the Stokes Raman output from nitrobenzene was also studied photometrically by using the polarization analysis procedure of Fig. 3. The exit window of the cell was imaged through a Fresnel rhomb and a Wollaston prism to form two images on a boron nitride surface. The images were monitored separately by silicon photodiodes through filters. Depending on the relative orientation of the Wollaston prism to the Fresnel rhomb, signals produced by the two images were proportional either to the right and left circular component intensities or to the intensities of the components linearly polarized parallel and perpendicular to the original laser polarization. When the cell was removed, the signals showed that only the nominal input polarization (either linear or circular) was present to within one part in 200, the limit of resolution. When Stokes light was produced by linearly polarized input, it was found to be linearly polarized to within one part in 200; when it was produced by a circularly polarized input, it was found to contain equal intensities of both circular polarizations and of both linear polarizations. These results applied over the entire power range where Stokes light could be observed (roughly seven orders of magnitude variation in Stokes output), and are consistent with the photographic observations. Also, apertures ranging from 1/2 to 5 mm in diameter placed in the laser beam did not affect these findings, even when the cell containing the liquid was placed in the far field of the 1/2 mm aperture.

D. Resolution of Anomalies in SRS

The observation of the self-trapping now associated with most SRS in liquids was a major step forward in the understanding of the SRS process in these media. We now discuss how well the concept of self-trapping can explain the anomalies which have been observed. The general conclusion is that the phenomenon satisfactorily explains some features, explains some other features in principle but not in detail, and leaves some questions still unanswered, even conceptually.

The most striking of the puzzling anomalies are the low thresholds and the large wavelength spreads with multimode pumping. These are also the features which have received the best explanations. The time-resolved observations of filaments in nitrobenzene discussed above showed that the low thresholds can be quantitatively explained as resulting from transient beam trapping. Bloembergen and Lallemand[11]

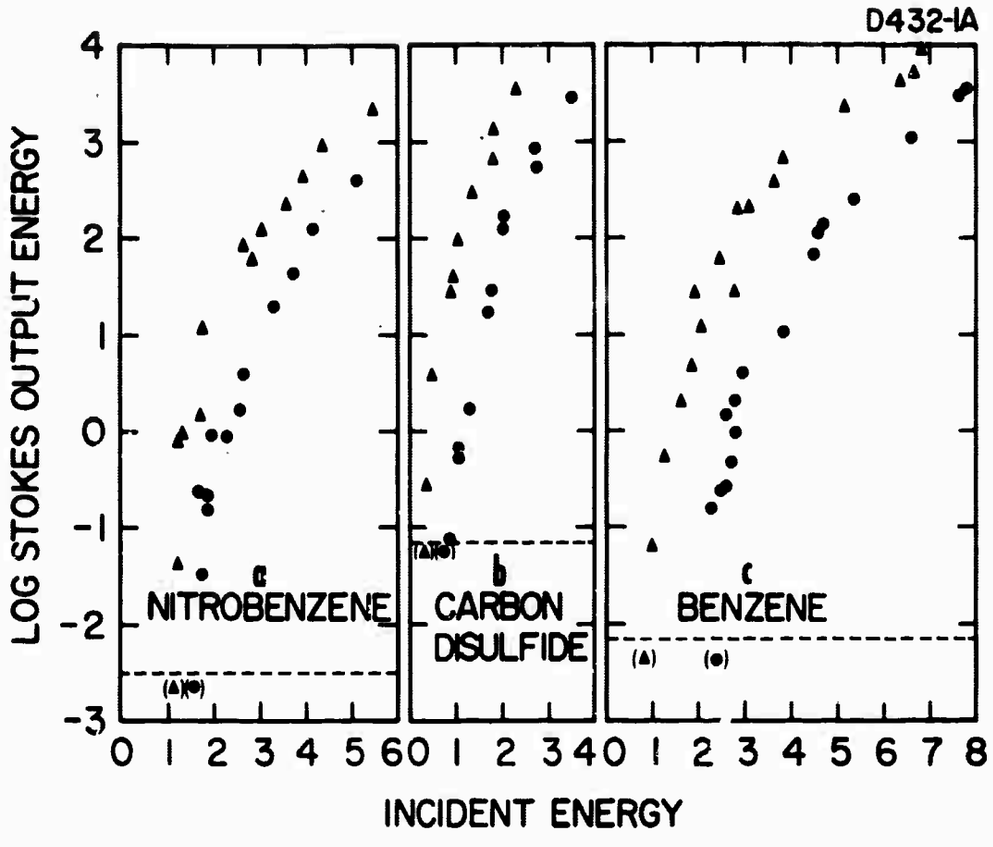

Fig. 4. Plots of the Raman Stokes output energy versus ruby laser energy incident on a 10 cm cell of (a) nitrobenzene, (b) carbon disulphide, and (c) benzene. Triangular points represent linearly polarized incident light, circular points represent circularly polarized light. The zero of the log Stokes output energy corresponds roughly to a conversion of 10^{-5} of the laser energy to Stokes energy. The incident energy was not calibrated absolutely. The dotted lines represent pulses producing no detectable Stokes output.

have shown that frequency broadening can be explained in terms of orientation effects in anisotropic molecules. These results were sufficiently qualitative that another, similar process may be found pertinent, just as we feel that orientation effects may not completely explain the beam trapping phenomenon. In any case, the frequency spreading is definitely related to the beam trapping.

The forward Stokes to backward Stokes ratio measurement is generally complicated by feedback to the ruby laser via stimulated Brillouin scattering (SBS). Also, the coupling to the anti-Stokes radiation is very important to the development of the Stokes radiation, and the former is not well understood.[2] Therefore, we must conclude that the forward-backward Stokes ratio is not completely understood, but we may hope it can be understood within present concepts. Essentially the same comment can be made regarding the importance of regeneration, the Stokes to anti-Stokes ratio, and the anti-Stokes emission angles. While the single-pass gain can be sufficiently large under trapped conditions to obtain the observed output from a single pass, the details of the frequency composition and coherence properties of the SRS-induced radiation are not well understood. Likewise, the anomalously large amount of anti-Stokes radiation produced and the "wrong" anti-Stokes emission angles have been shown by Garmire[12] and by Bret and Denariez[13] to be intimately associated with beam trapping, but the processes invovled are not at all well understood.

Probably the most pressing remaining questions concern SRS in gases. The observation by Terhune[14] of large amounts of anti-Stokes radiation in hydrogen gas, and the measurements by Mayer[15] of SRS conversion properties in hydrogen very similar to those observed in liquids showing beam trapping are extremely puzzling. There is no known process which could furnish a nonlinear index large enough to obtain beam trapping in these cases, and, as far as is known, nothing but beam trapping has the potential for explaining these effects. Thus, many questions remain open, and it appears that the investigation of gases and their comparison with liquids will be a very fruitful avenue of approach to understanding more about the complex SRS process.

E. Theory of Beam Trapping

1. Introduction

The "self-focusing" or "self-trapping" of the pump light or the Raman scattered light in a Raman laser tends to destroy the coherence of the Raman output. Therefore, self-focusing effects must be prevented if a high coherence high energy Raman output is to be obtained.

It is generally felt that index changes from electrostriction and heating which involve macroscopic mass transport in the Raman media will not develop significantly in times short compared with 10^{-7} - 10^{-8} sec. However, much faster-acting effects which do not involve macroscopic mass transport may cause index changes and self-trapping. The most studied of the fast self-trapping effects is that which arises from the reorientation of asymmetric molecules in the strong optical fields and is called the ac Kerr effect. The thresholds for self-trapping that are expected theoretically from the ac Kerr effect are in rough quantitative agreement with the observed thresholds in such asymmetric molecular liquids as CS_2, nitrobenzene, benzene, toluene, and benzoylchloride. These power thresholds lie in the 10 to 100 kW region, or, in terms of pulse energies, in the 10^{-3} - 10^{-4} J region. These threshold energy values give essentially an upper limit on the Raman output power that can be obtained in an undistorted wave train. Therefore, for the purposes of the present study, we would like to see if some Raman active liquids could be found which have three or more orders of magnitude higher trapping thresholds. One might hope that a perfectly symmetric molecule which can exhibit no ac Kerr effect might therefore have a trapping threshold (in liquid) many orders of magnitude greater than those liquids mentioned above. In this section we are concerned with the theoretical investigation of this possibility. The main result is that no such hope exists; that is, no Raman active liquid near room temperature can be expected to sustain a wave of around 10^6 W or greater without deterioration of beam coherence due to self-focusing effects.

If the main contribution to the fast-responding part of the nonlinear index of a liquid of symmetric molecules were a result of the nonlinear polarizability, perhaps an increase in trapping threshold powers of three or more orders of magnitude (10^7 to 10^{10} W) could be expected. However, there is another contribution to the nonlinear index which is much larger, being of the order of the reorientation contribution for asymmetric molecules, and remaining large for symmetric molecules. This contribution is from the local molecular redistribution in space that must occur in the presence of strong optical fields.

The probability of finding a certain spatial configuration of molecules in a liquid depends on the energy of that configuration. When a large optical field is present in the liquid, the relative energies of various configurations will change owing to the added dipole-dipole interactions. Configurations having the largest polarization become energetically more favorable and hence more probable, and an increase in the index of refraction, similar to that from reorientation, must result from the spatial redistribution. This can happen either with a macroscopic density change (electrostriction) and mass transport or without either. Here we compute the nonlinear index change from

microscopic redistributions which involve no macroscopic density changes in the liquids and hence can occur in times very short compared with a nanosecond pump pulse duration. It is such spatial redistribution which will determine the short-pulse self-trapping thresholds of fluids of symmetric molecules rather than electronic or electrostrictive effects. In fact, we will find that even for such asymmetric molecules as nitrobenzene and benzene redistribution effects are as important as the ac Kerr effect in self-trapping. Examination of the predicted relative thresholds of all liquids for which measurements have been made at Hughes or reported elsewhere show all behaving in accord with the estimates made below from combined reorientation and redistribution. For example, the symmetric molecule CCl_4 is predicted to have a lower threshold than the asymmetric molecules chloroform, acetone, acetic acid, and water, and a higher threshold than benzene, nitrobenzene, and toluene as is observed. It is further suggested that some other symmetric molecules such as tetraisopropyl lead which have not yet been studied experimentally will also self-trap light at thresholds as low as those at some asymmetric molecules which have exhibited the effect.

In the course of estimating the nonlinear index of liquids of symmetric molecules we derive a rigorous lower bound for the linear index within the framework of classical statistical mechanics. This quite strong inequality is of interest because it contradicts (by a very small amount) recent experimental results on argon, methane, CF_4, and other symmetric materials.[16]

2. Formulation

We calculate here the nonlinear dielectric constant as if the fields were static. The optical dielectric constant can be obtained from the static result simply by replacing the static polarizability by the optical polarizability since permanent moments have no effect on the optical properties. Also, the square of the static electric field must be replaced by the average over many cycles of the square of the optical field. That the intermolecular forces and molecular torques are essentially the same for optical as for static fields is because the motions of the molecules in the liquid cannot respond to the forces existing at optical frequencies, but only to the relatively low frequency components of force. The logic of the extension of the static results to the optical case will become clear in the following development. At the cost of considerable complexity, the development can in fact be made mathematically rigorous for optical fields throughout and achieve essentially the same result. However, the simpler treatment that is available for the nonlinear static dielectric constant will be pursued here because of its greater physical clarity.

To find the static dielectric constant, we compute the free energy $\mathcal{F}$ of an ellipsoidal sample placed in a uniform x-directed electric field E_o such that an axis of the ellipse is parallel to the field. Then the total electric dipole moment of the sample M is obtained from the well known relation (proved later)

$$M = - d\mathcal{F}/dE_o . \tag{1}$$

Because the sample is ellipsoidal and the external field uniform, the polarization per unit volume P inside the sample will be uni orm and x-directed. We assume the sample to have a fixed volume V. Therefore,

$$P = M/V . \tag{2}$$

We desire the nonlinear index only to second order in the electric fields so we compute $\mathcal{F}$ to fourth order in the fields and obtain a result of the form

$$\mathcal{F} = (bE_o^2/2 + c\, E_o^4/4)V \tag{3}$$

from which we have

$$P = b\, E_o + c\, E_o^3 . \tag{4}$$

In an ellipsoidal sample uniformly polarized along a principal axis, the relation of the polarization density to the macroscopic electric field E is generally written[2]

$$E = E_o - LP \tag{5}$$

where L is called the depolarization factor for that axis of the ellipsoid. The factor L can have values between 0 and 4π depending only on the shape of the ellipsoid.[17] If we define a linear susceptibility χ and a nonlinear susceptibility η by the relation

$$P \equiv \chi E + \eta E^3, \tag{6}$$

a comparison of (4) and (6) with the aid of (5) shows that

$$\chi = b/(1 - Lb) \tag{7}$$

and

$$\eta = c(1 - Lb)^{-4} = c(1 + L\chi)^4 . \tag{8}$$

The nonlinear dielectric constant ϵ_{NL} is

$$\epsilon_{NL} = 1 + 4\pi P/E = 1 + 4\pi (\chi + \eta E^2), \qquad (9)$$

and, in extrapolating our results to the optical case, we would therefore have an index of refraction n_{NL} given, to second order in E, by

$$n_{NL} = n + (2\pi/n)\, \eta \bar{E}^2 \qquad (10)$$

where $\bar{E}$ is the rms electric field averaged over many optical cycles and n is the linear index of refraction. Following the standard practice, we define a "nonlinear index" n_2 by

$$n_2 \equiv 2\pi\eta/n\,. \qquad (11)$$

The threshold power P_c required to begin trapping a smooth beam is[5]

$$P_c \approx (1.22\,\lambda_o)^2\, c_o/(128\, n_2) \qquad (12)$$

where λ_o and c_o are the vacuum wavelength and velocity of light respectively. We now have all the necessary relations to connect the nonlinear index effects with the electric free energy $\mathcal{F}$.

In computing the free energy $\mathcal{F}$, we assume that we are dealing with a classical fluid and use classical statistical mechanics. We must therefore formulate the total potential energy v of the N molecules in the sample when they are placed at positions $\underset{\sim}{r}^1, \ldots \underset{\sim}{r}^N$, have electric dipole moments $\underset{\sim}{m}^1, \ldots \underset{\sim}{m}^N$, and are oriented at the Euler angles which we symbolize by $\Omega_1, \ldots \Omega_N$.

We anticipate that the electronic nonlinearities will be small compared to those with which we are concerned, and assume that the internal energy v_γ of the γ^{th} molecule is quadratic in the components of its electric dipole moment $\underset{\sim}{m}^\gamma$. If m_a^γ are the components of this moment along the principal axes a = 1, 2, 3, of its polarizability ellipsoid, then[17]

$$v_\gamma = \frac{1}{2} \sum_{a=1}^{3} (m_a^\gamma)^2 / \alpha_a \qquad (13)$$

where $\alpha_1, \alpha_2, \alpha_3$ are the polarizabilities of the molecule along its principal axes. The components m_a^γ are related to the components m_i^γ measured in a laboratory-fixed coordinate system by*

*We will consistently use the subscripts a through h to denote the space components of a vector or matrix referred to the principal axes 1, 2, 3 of the polarizability ellipsoid fixed in the molecule. Subscripts from i onward always denote space components referred to axes fixed in the laboratory.

$$m_i^\gamma = R_{ia}(\Omega_\gamma) m_a^\gamma . \tag{14}$$

The repeated space indices here and elsewhere are assumed to be summed. The matrix $R_{ia}(\Omega_\gamma) = R_{ai}^{-1}(\Omega_\gamma)$ represents the rotation operator for the Euler angles Ω_γ of the γ^{th} molecule, and will be abbreviated R_{ia}^γ.

The interaction energy $v_{\gamma\mu}$ between two molecules at positions $\underset{\sim}{r}^\gamma$ and $\underset{\sim}{r}^\mu$ will be assumed to be[5]

$$v_{\gamma\mu} = v_{o\gamma\mu} + m_i^\gamma m_j^\mu D_{ij}^{\gamma\mu} \tag{15a}$$

where $v_{o\gamma\mu}$ is a hard core repulsive potential and the remaining term is the dipole-dipole interaction energy:

$$D_{ij}^{\gamma\mu} \equiv \frac{(\delta_{ij}\delta_{k\ell} - 3\delta_{ik}\delta_{j\ell})(r_k^\gamma - r_k^\mu)(r_\ell^\gamma - r_\ell^\mu)}{|\underset{\sim}{r}^\gamma - \underset{\sim}{r}^\mu|^5} . \tag{15b}$$

The m_a^γ may be taken to be the independent harmonic "internal" coordinates of the molecules which describe the electronic polarization. That is, it is appropriate to integrate over all values of these coordinates in evaluating the free energy from the potential energy function. The free energy $\mathcal{F}$ of the liquid in the external field may therefore be written

$$e^{-\beta\mathcal{F}} = \iiint d\{\underset{\sim}{r}\}\, d\{\Omega\}\, d\{m_a\}\, e^{-\beta v} \tag{16a}$$

where

$$v = \Sigma_\gamma(-\mu_x^\gamma E_o + v_\gamma) + \tfrac{1}{2}\Sigma_{\gamma,\mu} v_{\gamma\mu} \tag{16b}$$

is the total potential energy of a configuration of the positions, moments, orientations of the molecules. $\int d\{\underset{\sim}{r}\}$ symbolizes the integration $\int d\underset{\sim}{r}^1 \ldots \int d\underset{\sim}{r}^N$ over the entire volume V of the ellipsoid of every molecular position and similarly for all molecular orientations $\{\Omega\}$ and internal molecular coordinates $\{m_a\}$. β is defined as the inverse of (the temperature times Boltzmann's constant).

This completes the formulation of the static dipolar free energy suitable for classical liquids. The relations (1) through (12) connect the dependence of $\mathcal{F}$ on an externally applied electric field E_o with the threshold power for self-focusing or self-trapping which we wish to predict. It remains to carry through the evaluation of the free energy $\mathcal{F}$ starting from the basic definition (16).

3. A Variational Principle for Calculation

In order to obtain from (16) an accurate estimation of $\mathcal{F}$ for liquids it does not suffice to expand $\mathcal{F}$ in powers of the number density $\rho = N/V$. We are therefore going to employ a variational approach which obtains an upper bound for $\mathcal{F}$. Parameters will exist in the upper bound which can be varied to obtain a lowest upper bound within any approximation scheme.

To obtain a variational principle, we note that the total potential energy v is a quadratic function of the dipole moment coordinates m_a^γ. This means that if we define new coordinate variables of integration ν_a^γ by

$$\nu_a^\gamma = m_a^\gamma - \mu_a^\gamma \tag{17}$$

where the μ_a^γ are those values which minimize v for a given positional and orientational configuration, then we can rewrite (16) as

$$e^{-\beta\mathcal{F}} = \iint d\{\underset{\sim}{r}\}d\{\Omega\}\exp[-\beta\Sigma_{\gamma\mu} v_{o\gamma\mu} - \beta v' - \beta \min_{\{\mu\}} \phi] \tag{18}$$

where (see footnote on p.__)

$$\phi \equiv \phi(\{\underset{\sim}{\mu}\}, \{\underset{\sim}{r}\}, \{\Omega\}, E_o)$$

$$\equiv \Sigma_\gamma \left(\frac{-\mu_x^\gamma E_o + \frac{1}{2}\Sigma_a \mu_a^{\gamma 2}}{\alpha_a + \frac{1}{2}\Sigma_\nu \mu_i^\gamma \mu_j^\nu D_{ij}^{\gamma\nu}} \right) \tag{19}$$

is the function which is minimized by our choice of the μ_a^γ and

$$\exp[-\beta v'(\{\underset{\sim}{r}\},\{\Omega\})] \equiv \int d\{\nu_a\} \exp[-\tfrac{1}{2}\beta\Sigma_\gamma(\nu_a^{\gamma 2}/\alpha_a + \Sigma_\mu \nu_i^\gamma D_{ij}^{\gamma\mu} \nu_j^\mu)]. \tag{20}$$

The symbol $\{\underset{\sim}{\mu}\}$ represents the set of all values of the μ_a^γ. The intermolecular potential v' defined by (20) cannot depend on the electric field E_o (or the $\{\underset{\sim}{\mu}\}$ would not minimize ϕ) and represents, of course, the long range van der Vaal's potential due to induced dipole-induced dipole interactions. This potential has been analyzed in the literature[17] and we need not discuss it further here.

It is too difficult to find an exact explicit expression for $[\min_{\{\mu\}} \phi]$, but if we insert wrong values for the $\{\underset{\sim}{\mu}\}$ into ϕ we at least obtain an estimate for the field-dependent part $\mathcal{F}_E$ of $\mathcal{F}$ that is too high. We therefore have the useful inequality that for any $\{\underset{\sim}{\mu}\}$ whatever

$$\mathcal{F}_E \leq F \tag{21}$$

where

$$e^{-\beta F} \equiv \iint d\{\underset{\sim}{r}\}\, d\{\Omega\}\, w(\{\underset{\sim}{r}\}, \{\Omega\}) e^{-\beta\phi} \tag{22a}$$

and

$$w \equiv \frac{\exp(-\beta \Sigma_{\gamma\mu} v_{o\gamma\mu} - \beta v')}{\int d\{r\}\, d\{\Omega\}\, \exp(-\beta \Sigma_{\gamma\mu} v_{o\gamma\mu} - \beta v')} . \tag{22b}$$

With this inequality we may proceed with a variational calculation of the desired field dependent part $\mathcal{F}_E$ of the free energy.

4. The Effective Field Approximation

We will use a local field approximation in which we use the approximate values

$$\mu_a^\lambda = \alpha_a R_{xa}^\gamma E' \tag{23a}$$

or equivalently

$$\mu_j^\gamma = R_{ja}^\gamma \alpha_a R_{xa}^\gamma E' \tag{23b}$$

as if each molecular moment saw only an effective x-directed local field of magnitude E'. We will then adjust E' to minimize the resulting upper bound F for the free energy (calculated to fourth order in E'). The F thus obtained is a function of the shape of the ellipsoidal sample, but the dielectric constant derived from it via (9) is not. (Otherwise we could vary the shape parameters to improve further the accuracy of the estimate for the dielectric constant.) Using (23) in (19) gives

$$e^{-\beta F} = \ll e^{-\beta(u_2 - u_1)} \gg \qquad (24)$$

where

$$u_1 \equiv \Sigma_\gamma \underset{\sim}{G} \cdot \underset{\sim}{\alpha}^\gamma \cdot \underset{\sim}{E}' , \qquad (25a)$$

$$\underset{\sim}{G} \equiv \underset{\sim}{E}_o - \underset{\sim}{E}'/2 , \qquad (25b)$$

and

$$u_2 \equiv \tfrac{1}{2}\Sigma_{\gamma,\nu} \underset{\sim}{E}' \cdot \underset{\sim}{\alpha}^\gamma \cdot \underset{\sim}{D}^{\gamma\nu} \cdot \underset{\sim}{\alpha}^\nu \cdot \underset{\sim}{E}' . \qquad (26)$$

We have introduced the usual shorthand notation for multiplication among the 3 x 3 space matrices

$$\underset{\sim}{\alpha}^\gamma \equiv R_{ia}^\gamma \alpha_a R_{ja}^\gamma , \quad \underset{\sim}{D}^{\gamma\nu} \equiv D_{ij}^{\gamma\nu} ,$$

and the three-vectors $\underset{\sim}{E}_o = \hat{x}\, E_o$ and $\underset{\sim}{E}' = \hat{x}\, E'$. The double average brackets $\ll \quad \gg$ in (24) symbolize the integrations over $\{\underset{\sim}{r}\}$ and $\{\Omega\}$ weighted by $w(\{\underset{\sim}{r}\})$ which is normalized so that $\ll 1 \gg = 1$. We will often use only the single average bracket when either the angle or position average is required alone; which average is intended will be clear from the context. In either case, $\langle 1 \rangle = 1$.

We expect (as we will find) that the best local field E' will be of the order of E_o. Therefore, eq. (24) implies that, to fourth order in E_o, F is given by

$$F = U_2 - U_1 - \frac{\beta}{2}[U_{22} - 2\,U_{12} + U_{11}] \qquad (27)$$

where

$$U_i \equiv \ll u_i \gg \qquad (28a)$$

and

$$U_{ij} \equiv \ll u_i u_j \gg - \ll u_i \gg \ll u_j \gg : \; i,j = 1,2 . \qquad (28b)$$

The integrals in U_1 and U_{11} are easily performed to give

$$U_1 = N\alpha G E' \tag{29}$$

and

$$U_{11} = N G^2 E'^2 \Delta^2 \alpha^2 \tag{30}$$

where the dimensionless anisotropy parameter Δ is defined by

$$\Delta^2 \equiv 2[(a_1 - a_2)^2 + (a_2 - a_3)^2 + (a_1 - a_3)^2]/(45\,\alpha^2) \tag{31}$$

and $\alpha \equiv (a_1 + a_2 + a_3)/3$ is the usual linear molecular polarizability.

To perform the integrals in U_2 and U_{12} we require the positional average of $D_{xx}^{\gamma\mu}$. If the dimensionless two-particle correlation function defined by

$$p(r_{12}) \equiv V^2 \, d\underset{\sim}{r}_3 \ldots d\underset{\sim}{r}_N \, w(\{\underset{\sim}{r}\}) \tag{32}$$

approaches a constant value when $r_{12} \equiv |\underset{\sim}{r}_1 - \underset{\sim}{r}_2|$ is still small compared with the size of the liquid sample under consideration, then it is well known that (neglecting terms of order N^{-1} smaller) the required positional average gives [17]

$$\langle \Sigma_{\gamma,\mu} D_{xx}^{\gamma\mu} \rangle = N\rho\ell \tag{33}$$

where

$$\ell \equiv L - 4\pi/3 , \tag{34}$$

independently of the form of $p(r)$.[17] ρ is the number density of molecules N/V, L is the depolarizing factor along the principal axis of the ellipsoidal sample which is parallel to the external field. Therefore

$$U_2 = N\alpha^2 E'^2 \rho\ell/2 \tag{35}$$

and

$$U_{12} = N\alpha^3 G E'^3 \rho\ell \Delta^2 . \tag{36}$$

To perform the integrals required in U_{22}, the exact form of the two, three, and four particle correlation functions is required. For purposes of calculation, we have assumed that $p(r)$ is a simple step function which properly normalized is

$$\begin{aligned} p(r) &= 0, \qquad r < d \\ &= (1 - \tau/V)^{-1}, \quad r > d \end{aligned} \tag{37a}$$

where

$$\tau \equiv 4\pi d^3/3 . \tag{37b}$$

We have used the usual "Kirkwood superposition approximation" for the three- and four-particle correlation functions, expressing them in terms of $p(r)$. The details of the calculation of U_{22} with these approximations is given in Appendix IV; the result is

$$\begin{aligned} U_{22}/(NE'^4 \rho^2 a^4) &= (l^2 + 2\pi^2/3)\,\Delta^2 + 2\pi^2/3 \\ &+ \pi^2(32 + 136\,\Delta^2 + 167\,\Delta^4)/(45\,\rho\tau) \\ &+ 0.961\,\rho\tau\,(1 + K_4/4) \end{aligned} \tag{38}$$

where K_4 is a small contribution ($\sim 10^{-1}$) from an integral that we have not been able to evaluate exactly and which we may neglect without affecting the probable accuracy of the over-all results.

5. The Best Effective Field-Linear and Nonlinear Index Formulae

Having explicit expressions for all the terms in (27) for F, we will adjust the magnitude E' of the effective local field to obtain as low a value as possible for the upper bound F of the free energy. Since the terms of order E_o^4 are supposed to be orders of magnitude smaller than those of order E_o^2, it is easily seen that the best E' is that which minimizes the terms of E_o^2. Any small change of E' from such a value raises these large terms more than it can depress the smaller terms of order E_o^4. That is, we need only minimize $(U_2 - U_1)$ with respect to E' and find

$$E' = E_o/(1 + \rho a l) \tag{39}$$

is the best choice. Using (39) in (27) gives immediately the approximate b and c coefficients of (7), from which, with the aid of (7) through (12), the following relations result for the linear dielectric constant ϵ and the nonlinear index n_2:

$$\epsilon \geq \frac{1 + 8\pi\rho a/3}{1 - 4\pi\rho a/3}$$

and

$$n_2 \approx \frac{\pi\rho a^2\beta}{n(1 - 4\pi\rho a/3)^4}\left[\Delta^2 + \frac{4\pi^2\rho a^2}{45\tau}(32 + 136\,\Delta^2 + 167\,\Delta^4)\right.$$

$$\left. + \frac{8\pi^2\rho^2 a^2(1 + \Delta^2)}{3} + 3.843\,a^2\rho^3\tau\right]. \qquad (41)$$

We reiterate that the estimate (41) of the nonlinear index does not contain any effects of macroscopic density change or current in the fluids, but presumably does represent the steady state effects of all microscopic molecular reorientation and redistribution.

6. Discussion and Examination of Accuracy

The inequality (40) is equivalent to the statement that the Clausius-Mossotti function $(\epsilon - 1)\rho^{-1}(\epsilon + 3)^{-1}$ is always larger than $4\pi a/3$ for a classical fluid of molecules of fixed linear polarizability, regardless of the intermolecular forces, provided that the two-particle correlation function depends only on the intermolecular spacing and becomes constant for large spacing. The fact that many fluids have been found which slightly disobey (40) demonstrates that at least one of these assumptions is not entirely valid.[16] However, the observed deviation of the Clausius-Mossotti function from $4\pi a/3$ is rarely more than a few percent and this suggests that our nonlinear term (41) might be accurate to within 10 to 50%, depending on the molecule. However, unlike ϵ, n_2 is very sensitive to the form of the two-, three-, and four-particle correlation functions, and the errors that result from approximating the latter with the Kirkwood approximation are completely unknown at present. Nevertheless, it is reassuring that certain features of (41) are familiar. The first term in the brackets on the RHS is exactly the formula of Debye[18] for the dc nonlinear dielectric constant (except we are extending it to optical frequencies). This term dominates all others at low densities. The other terms are all proportional to higher powers of the density than this term and represent high density corrections which will be important in liquids.

Several terms in (41) require knowledge of the molecular volume $\tau/4$. This parameter also occurs in the theories of the fluid viscosity, the heat conductivity, and the virial coefficients. An examination of data on representative fluids in each of these categories gives values for τ which vary typically by 10% in a given fluid. Data are not available for all of the fluids of interest to us, but in those where it is available, τ is always within $\pm$ 10% of $2.5/\rho$. Therefore, we have used this value for τ for all liquids in numerical calculations of the indices. The nonlinear indices n_2 predicted by (41) are listed in Table I for those liquids whose nonlinear effects have been commonly studied. The table also includes several symmetric-molecule liquids whose nonlinear indices are predicted to be comparable with the most nonlinear asymmetric-molecule liquids. However, the molecules in these liquids are likely to be so large that our model of hard spheres interacting as if point dipoles were at their centers breaks down. The values of n_2 for these molecules are therefore intended to be suggestive of possible effects.

With the improvement in our approximations when applied to the smaller molecules and from comparing our results with available data, we expect that our tabulated values for n_2 (for these smaller molecules) should have a relative accuracy of perhaps $\pm$ 20% or better. The absolute accuracy is difficult to judge because of the uncertainties in the Kirkwood approximation.

Included in Table I, along with our estimates of n_2 and P_c, is the nonlinear index n_2^o which would result from the low density theory[18] of Debye which neglects the effects of molecular redistribution. The Debye index n_2^o is always smaller than that of our (41). Even considering the large possible errors in (41), one is led to conclude that reorientation effects on the index are not much more important than redistribution effects, and often contribute negligibly to the change in index.

In addition, the recent experimental results of Mayer for two thirds of the difference between the nonlinear indices parallel and perpendicular to the applied field[15] are given in the table. If molecular reorientation were the dominant mechanism and the Debye theory[18] correct, this number would equal n_2.

Also included in Table I are the recent experimental results of Wang and Racette[7] for a coefficient c_{1221} which expresses the nonlinear tendency of the liquid to rotate the axes of the polarization ellipse of the incident light. If molecular orientation were dominant and the Debye theory[18] correct, the numbers in this column would also equal n_2.

Unfortunately, our theory of the nonlinear index is only for the change in index for light polarized parallel to a strong plane polarized beam. When the theory is extended to two beams of different polarization, the ideas about molecular redistribution can be checked

TABLE I

Some Nonlinear Optical Coefficients for 21 Liquids*

Liquid	$n_2^o \times 10^{12}$ calc. from Ref. 18	$n_2 \times 10^{12}$ calc. from eq. (47)	$\frac{2}{3} 10^{12} (n_2 - n_{2\perp})$ measured, Ref. 15	$10^{12} \times 16\pi c_{1221}/n$ measured Ref. 19	P_c(kW) calc. for 6943 Å
1. Lead tetraisopropyl[a]	0	111			1.51
2. Tin tetra 2-metholbutyl[a]	0	109			1.54
3. Tin tetrapental[a]	0	108			1.55
4. CS_2	22	96	13.6	10.5	1.74
5. Tin tetralbutyl[a]	0	89			1.88
6. $Si Br_4$[a]	0	82			2.05
7. Lead tetraethyl[a]	0	81			2.07
8. Benzoylchloride		73[b]	7.9		2.31
9. Nitrobenzene	8.8	69	9.4	6.8	2.43
10. Bromobenzene	6.4[c]	68			2.47
11. Acetophenone		56[d]			3.10
12. Chlorbenzene	6.3	54			3.11
13. Toluene	5.6	45	3.0	2.7	3.77
14. Benzene	4.4	37	1.3	2.2	4.5
15. $C Cl_4$	0	24	1.7		7.1
16. Chloroform	1.3	19	0.54		9.0
17. Water		11[b]	0.1		15.4
18. Acetone	0.6	6.7	0.2		25.5
19. Acetic acid		5.7[b]	0.4		30
20. Liquid CH_4	0	3.0			56
21. Liquid H_2	0.010	0.024[e]			7000

*The values of n_2^o are calculated from the standard relation of (18) for the effect of reorientation of asymmetric molecules. The n_2 are calculated from (47) and include redistribution as well as reorientation effects. The $2/3(n_2 - n_{2\perp})$ are the values of optically induced birefrigence measured by Mayer[15] and would equal n_2 if the reorientation theory[18] were valid. The $16\pi C_{1221}/n$ were measured by Wang and Racette[19] and would equal n_2 if the reorientation theory were valid. The critical powers for self-trapping are computed using our calculated values for n_2 in (12). The liquids are given in the nominal order of the P_c. The accuracy of the given results is discussed in the text and is less than indicated by the figures given here. The polarizability data used in the computations are from Ref. 20.

[a]Purely symmetric molecule.

[b]Estimated by adding value from column 3 to n_2 calculated with $\Delta = 0$.

[c]Estimated by scaling Table 142072 in Ref. 20 to Table 142071.

[d]Estimated by assuming molecule is symmetric ($\Delta = 0$).

[e]This value is less accurate than others in column because H_2 exhibits quantum effects which we have ignored.

by direct comparison with the results of Mayer[15] and of Wang and Racette.[19] This extension is planned.

7. Conclusions

The results of (41) as expressed in Table I indicate that no room temperature liquid can be expected to support a coherent beam of as much as a megawatt for many diameters of path length without significant beam deterioration occurring. Even liquid hydrogen, which has a much lower expected nonlinear index than normal liquids, would not be expected to support beams of much over 10^7 W without self-focusing effects. However, we note the following points which may bear on, or modify, the predicted critical powers of Table I and hence may modify the conclusions.

First, the first quantitative measurements of power thresholds for self-trapping in benzene, nitrobenzene, and toluene[9], and in CS_2 (Ref. 10) have given thresholds an order of magnitude greater than those predicted in Table I. However, Garmire, Chiao, and Townes (private communication) have recently seen "small scale" trapping which sets in at an as yet undetermined power level somewhat lower than that which they reported in Ref. (10). Therefore, the size of the discrepancy, if any, between our predicted thresholds and those observed is still uncertain.

Secondly, as Bloembergen and Lallemand have pointed out, the time delay for some molecules to reorient themselves in a suddenly applied large electric field may not be small compared with the typical duration of a laser pulse.[8] This suggests that if the powers used in the previous measurements of thresholds were kept on longer, the thresholds might have been lower. That is, longer laser pulses may be required if the "steady state" nonlinear index we have calculated is to be achieved. Crude estimates of this relaxation time made on the basis of the classical Debye theory indicate that liquids having a viscosity greater than or of the order of one poise might encounter this raising of threshold. The liquids of Table I are less viscous than this by an order of magnitude or more.

Third, stimulated Brillouin scattering may have a threshold lower than that for self-trapping and complicate matters in a way which spoils further the coherence of any Raman laser action.

Also, the question of how the turbulence and vibrational waves which exist in liquids under the normal conditions in which experiments are performed, affects the threshold for self-focusing has never been answered. Small bubbles and impurities may also have some effect. All such effects would probably raise the threshold for producing observable self-focusing above the apparently low predictions in Table I of (41).

BLANK PAGE

IV. SUMMARY

The self-focusing or self-trapping of the pump light or the Raman scattered light in a Raman laser tends to destroy the coherence of the Raman output. Therefore, self-focusing effects must be understood and probably prevented if a high coherence, high energy Raman output is to be obtained. Our experimental studies of stimulated Raman scattering and the concomitant beam trapping have demonstrated the following points.

Although the time-integrated intensities of observed filaments formed in the laser beam by a Raman-active liquid are not nearly high enough to explain the observed anomalously low SRS thresholds, the instantaneous intensities we have observed by time-resolved photographic techniques are indeed high enough. A given ruby and Raman filament never seems to persist for more than a small fraction of the laser pulse duration; different filaments, however, occur at different times during the pulse. The "gain anomaly" is therefore resolved, at least for the present, in the commonly studied liquids — CS_2, benzene, nitrobenzene, and toluene.

If, as is commonly supposed, a molecular reorientation were mainly responsible for the nonlinear index and for self-trapping in the Raman-active liquids, a simple theory we developed suggests that a circularly polarized plane input wave should exhibit a threshold for self-trapping four times that of a linearly polarized wave. Our experimental efforts to check this ratio showed that, in fact, a stable mode of propagation does not exist for any state of polarization except linear in CS_2, nitrobenzene, and presumably many other liquids as well. As soon as self-trapping in a circularly polarized beam was observed, the trapped light was seen to be depolarized. We have explained this behavior qualitatively, and expect it to occur for any known physical mechanism which can cause a nonlinear index, except electrostriction. We therefore conclude that electrostriction, often proposed as a mechanism for self-trapping, is unlikely to be a major factor in self-trapping in many liquids. However, we were not able to conclude anything about the reorientation hypothesis from our observations.

Our theoretical studies of beam trapping and its relation to SRS have been mainly devoted to understanding how self-trapping could be eliminated or at least made tolerable. To this end it was important to ascertain the relative importance of various physical mechanisms in creating a nonlinear index in various situations. We devised a self-trapping threshold ratio test and computed the expected ratios for different mechanisms. When observed instability in the propagation of nonlinearly polarized light made this test infeasible, we could only infer that electrostriction was not a dominant mechanism.

We therefore made a statistical mechanical calculation of the nonlinear index which assumed that no macroscopic density changes occurred, such as might occur from electrostriction or heating. It was hoped that molecules with no asymmetry of polarizability would show only the very small electronic nonlinearities in their dielectric behavior. This hope proved in vain, because the calculations showed that molecular redistribution in space would cause nonlinearities comparable with those caused by reorientation of very asymmetric molecules. We conclude, therefore, that no room temperature liquid will ever be likely to sustain a high energy Raman output beam without its nonlinear dielectric properties significantly distorting the beam. We look to gases as the most promising avenue for further investigations of the high energy, high coherence potential of Raman lasers.

References

1. D. Weiner, S. E. Schwarz, and F. J. McClung, J. Appl. Phys. 36, 2395 (1965).

2. F. J. McClung, W. G. Wagner, and D. Weiner, in Physics of Quantum Electronics, P. L. Kelley, B. Lax, and P. F. Tannenwald, Eds. (McGraw-Hill, New York, 1966), pp. 155-158.

3. G. A. Askan'yan, Zh. Eksperim. i Teor. Fiz. 42, 1567, translation, Soviet Phys. — JETP 15, 1088 (1962).

4. V. I. Talanov, Izvestia Uchebnykh Zavedenii Radiofizika 7, 564, Issue 3 (1964).

5. R. Y. Chiao, E. Garmire, and C. H. Townes, Phys. Rev. Letters 13, 479 (1964).

6. N. F. Pilipetskii and A. R. Rustamov, Soviet Phys. — JETP Letters 2, 55 (1965).

7. Y. R. Shen and Y. J. Shaham, Phys. Rev. Letters 15, 1008 (1965).

8. P. Lallemand and N. Bloembergen, Phys. Rev. Letters 15, 1010 (1965).

9. C. C. Wang, Phys. Rev. Letters 16, 344 (1966).

10. E. Garmire, R. Y. Chiao, and C. H. Townes, Phys. Rev. Letters 16, 347 (1966).

11. N. Bloembergen and P. Lallemand, Phys. Rev. Letters 16, 81 (1966).

12. E. Garmire, in Physics of Quantum Electronics, P. L. Kelley, B. Lax, and P. E. Tannenwald, Eds. (McGraw-Hill, New York, 1966), p. 167.

13. G. B. Bret and M. M. Denariez, Appl. Phys. Letters 8, 151 (1966).

14. R. W. Terhune, Solid State Design, November, 1963, p. 38.

15. G. Bret, F. Gires, and G. Mayer, Paper 2A-7, Fourth International Quantum Electronics Conference, Phoenix, Arizona, April 1966.

16. C. M. Knobler, C. P. Abiss, and C. J. Pings, J. Chem. Phys. 40 2200 (1964).

17. For complete reviews and bibliographies of electrostatics, dielectrics and classical statistical mechanics, see, for example, W. F. Brown, Jr., in Handbuch der Physik, Vol. XVII (Springer-Verlag, Berlin, 1956); or J. O. Hirschfelder, C. F. Curtiss, and R. B. Bird in Molecular Theory of Gases and Liquids (Wiley and Sons, New York, 1954).

18. P. Debye, in Marx's Handbuch der Radiologie VI (Leipzig, 1925), p. 768.

19. C. Wang, and W. Racette, paper presented at the Fourth International Quantum Electronics Conference, Phoenix, Arizona, April 1966.

20. Landolt-Börnstein, Zahlenwerte und Functionen I/3 (Springer-Verlag, Berlin, 1962), p. 509.

Appendix I

Reprinted from IEEE TRANSACTIONS ON *QUANTUM ELECTRONICS*
Vol. QE-1, Number 2, May 1965
Pp. 94-99

Longitudinal Mode Control in Giant Pulse Lasers

F. J. McCLUNG AND D. WEINER

***Abstract*—We have introduced longitudinal mode selection into a giant pulse laser to obtain single mode output from the laser. Some advantages of achieving longitudinal mode control in a giant pulse laser are noted. The methods of mode control used are described. These include orienting various reflecting surfaces in the laser cavity, cooling the ruby laser crystal, and introduction of a saturable dye in the cavity. Methods of measuring the mode structure are given. Results of these measurements with varying degrees of mode control are described in detail. Under some conditions it is possible to obtain essentially single mode behavior from the giant pulse laser.**

Introduction

THE FREQUENCY SPREAD of the output of a rotating prism giant pulse ruby laser (GPL) is typically about one Angstrom at room temperature. Closer examination shows this output to consist of many spectrally sharp components. These components are spaced, as may be expected, by frequencies equal to the reciprocal of twice the transit time between various pairs of reflecting surfaces in the laser cavity.

For many reasons it would be advantageous to reduce the spread in frequencies as much as possible so that ultimately only a single longitudinal mode of the laser cavity is operating. This would make it possible to observe small frequency shifts in experiments, such as Brillouin scattering or Rayleigh scattering. If the total output can be held essentially constant (as has been found possible), one would have a higher spectral brightness. This in turn would imply enhanced nonlinear effects in systems whose natural frequency spread is smaller than that of the GPL as would be the case for stimulated Raman scattering (SRS) in gases or for nonlinear optical effects in low-density plasmas. Also, the comparison of theory and experiment is much easier for a single mode laser pump for such processes as SRS. Here, for example, multimode theory [1] is qualitative in predicting the complex characteristics of anti-Stokes radiation for a multimode pump. Finally, it is sometimes possible to observe deep (~50 per cent) temporal modulation of the GPL pulse corresponding to mode spacings of the cavity. Thus, mode control techniques offer insights into methods of pulse shaping at these high frequencies.

We have achieved single mode behavior by a combination of techniques. These include carefully orienting various reflecting surfaces in the laser cavity, cooling of the ruby laser crystal, and introduction of a saturable dye in the cavity. We shall describe these techniques in detail and also discuss methods of measuring the mode structure in what follows.

Manuscript received February 10, 1965.
The authors are with Hughes Research Lab., Malibu, Calif.

Techniques of Mode Control

Figure 1 shows a schematic diagram of the apparatus used for longitudinal mode selection. The choice and arrangement of the elements are by no means unique; they are in part determined by such considerations as the availability of optical flats of suitable thickness and index of refraction, the availability of suitable optical

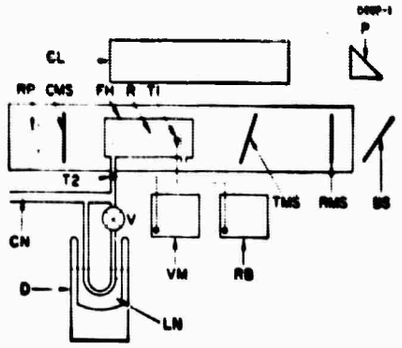

Fig. 1. An experimental arrangement for longitudinal mode control of a giant pulse laser showing gas laser (GL), prism (P), beam splitter (BS), reflection mode selector (RMS), transmission mode selector (TMS), ruby (R), flashlamp housing (FH), cryptocyanine mode selector (CMS), rotating prism (RP), thermistor (T1), thermocouple (T2), resistance bridge (RB), voltmeter (VM), valve (V), liquid nitrogen (LN), compressed nitrogen (CN), and Dewar (D).

coatings and the constraints imposed by the dimensions of the existing GPL. We make no effort here to determine the influence on our results of deviation from flatness or parallelism in the various optical elements. The ruby is usually poor (2λ at the best for our ruby), and our optical flats are finished to approximately λ/10 and parallel in transmission to λ/10.

In the future this mode-selected laser may well be made simpler. However, the present apparatus is sufficient to produce essentially single mode output with a power approximately that of a nonmode-selected GPL. It also serves well to illustrate the various methods for mode selection.

Reflection Mode Selection

Without longitudinal mode selection a typical GPL has a linewidth of ~1 — cm^{-1} which corresponds to ~150 modes for a 50-cm laser cavity. By replacing the front reflector of the GPL with a suitable optical flat we may modulate the mode structure so as to greatly reduce the number of oscillating modes as first reported by Stoicheff [2].

Our reflection mode selector (RMS in Fig. 1) is a ~2-mm-thick interferometrically flat and parallel sapphire plate ($n = 1.75$). The spacing between modes of this flat is 1.4 cm^{-1}. Hence, if one reflection maximum is centered on the peak of the R_1 line in ruby, the gain at the adjacent reflection maxima should be insufficient to produce oscillation. In this way the number of possible cavity modes is reduced from ~150 to ~20.

The reflection mode selector is aligned parallel to the uncoated ruby (R) and rotating prism Q switch (RP) with the aid of a gas laser alignment light source (GL) whose beam enters the laser cavity via a prism (P) and a beam splitter (BS). As far as mode selection is concerned, alignment of the surfaces by superposition, in the far field, of reflections from the various surfaces is almost as good as alignment by observing interference effects in reflected light from the gas laser. However, the latter method seems to give a higher power output.

The center of the R_1 line is tuned to a reflection maxima of the reflection mode selector by cooling the ruby. In our apparatus the ruby is cooled to about 0°C. This cooling is advantageous in other ways. It produces a decrease in the width of the R_1 line which further reduces the number of possible modes. It also increases the peak gain for the R_1 line. This is useful because the peak reflectivity of the reflection mode selector, whose refractive index was as high as was readily available, was only ~25 per cent, without the added reflectivity from the ruby.

The cooling is accomplished by passing cold dry nitrogen gas past the ruby crystal. Compressed dry nitrogen (CN) is passed into the flash lamp housing (EH) and past the ruby. Part of this nitrogen has been previously diverted through a heat exchanger that is in contact with liquid nitrogen (LN) in a Dewar (D). The amount of cooled nitrogen and hence the temperature of the gas mixture reaching the ruby is controlled by a valve (V). The inlet temperature of the gas is monitored by a copper-constantan thermocouple (T2) whose voltage is read on a microvoltmeter (VM). The temperature of the ruby is monitored by a thermistor (T1) whose temperature is determined by the current imbalance in a resistance bridge (RB).

We wish to temperature-tune the ruby so that its fluorescence peak coincides with a reflection maximum of the sapphire-plate mode selector. Near room temperature, we can accomplish this by observing the mode structure with a Fabry-Perot interferometer at a series of ruby equilibrium temperatures spaced 1° or 2° apart. For two of these temperatures differing by about 10°, the output of the GPL, measured with low resolution, consists of two modes of equal intensity spaced 1.4 cm^{-1} apart. The desired operating temperature is halfway between these two temperatures. At temperatures close to 0°C, it is better to determine the proper temperaure by high resolution observation of the GPL output.

To reduce the number of oscillating modes still further, one may introduce other sets of interferometrically flat surfaces within the laser cavity. These have transmission maxima and minima whose frequency spacing is determined by the distance between the surfaces and by the refractive index of the intervening material.

The ruby crystal provides one such set of surfaces. Our 3-in.-long ($\frac{3}{8}$-in. diameter) ruby has transmission maxima every 1.2 Gc. Thus it will suppress two or three out of every four consecutive cavity modes that are separated by 300 Mc. What remains then is to suppress all but one of the approximately five modes of the ruby which are separated by 1.200 Gc. This may be done, in principle, by placing the ruby at such a distance from another reflecting surface so as to form a suitable cavity. This may well have been done, intentionally or otherwise, in other experiments where mode control has been achieved.

The total effect of placing sets of reflecting surfaces

parallel to others in the laser cavity is, of course, very complex. Each surface forms a resonator with any other surface, thus giving a multitude of interacting resonant cavities of different frequencies. The net output spectrum of the system will also depend upon the reflectivities of the various surfaces and the gain of any material in the cavity. In order to gain more intuition concerning the problem, Wagner [3] of this laboratory performed computer calculations to find the minimum gain necessary for oscillation for many consecutive modes in a system consisting of a roof prism, a ruby, a glass reflection mode selector, and a 15-per cent end reflector. These calculations show that the position of the ruby and the resonances of the roof prism are relatively unimportant. They also show that the resonances of the ruby (perhaps due to its gain) and the position and thickness of the glass reflection mode sector are important. These observations help in choosing our initial cavity configuration. However, in our present configuration (Fig. 1) we find that the position of the ruby is important as it forms, with the reflection mode selector, an effective reflector of sufficient reflectivity to produce oscillation.

Transmission Mode Selection

Because of the physical limitations in our existing GPL, it is not possible to position the ruby to suppress all but one of the 1.2-Gc modes. To perform this task we insert an optically flat and parallel glass plate that is tilted slightly with respect to the laser beam. We can understand the operation of this mode selector by considering that this tilted plate has no reflection loss for frequencies corresponding to its Fabry-Perot transmission maxima. At other frequencies the reflections from this mode selector are lost from the cavity and thus constitute a frequency-dependent loss mechanism at a given angle. The fact that the plate is tilted means that there are no other resonators formed with other reflectors in the cavity. The frequency is tuned by varying the tilt of the flat.

The transmission mode selector (TMS) used is a 1-cm-thick interferometrically flat piece of flint glass whose modes are separated by ~10 Gc. The correct angle of tilt is determined empirically, i.e., by seeing which of several angles gives the least number of 1.2-Gc modes and mode interaction due to the 1-cm flat. The relative angle of tilt is determined by observing the deviation angle of the gas laser beam upon reflection from the flat. The use of this mode selector also has the advantage of suppressing weak side modes of the reflection mode selector which otherwise could have appeared at high pumping levels.

Dye Mode Selector

At the high power levels desired (~10 MW), the foregoing techniques may prove insufficient to produce reliable single mode behavior. Hence, one may add a cell containing a cryptocyanine dye solution to the foregoing configuration as had been shown useful in mode control [4]. The cryptocyanine mode selector (CMS) we use is formed by a $\sim 5 \times 10^{-6}$ molar solution of cryptocyanine in methanol placed in a cell with interferometrically flat windows 2 mm apart. Its absorption at 6943 Å is ~25 per cent. The cell is wedged and tilted slightly with respect to the laser beam to reduce transmission mode selection effects.

Measurement of Mode Structure

Our primary method of observing the mode structure of our GPL is with Fabry-Perot interferometers. For low-resolution studies we use a 2.4-mm separation between interferometer plates. For high-resolution work the spacing is 20 mm between plates which gives an interorder separation of 7.5 Gc. Each plate is flat and parallel to 1/80 wavelength, is coated with silver to a transmission of ~1 per cent, and is ~2 cm in diameter. The instrument is used with a camera of 1-m focal length. The resolution with the 2-cm spacer is ~200 Mc.

Some information about the mode structure can be obtained from the temporal modulation of the GPL output. This is observed with a biplanar photodiode and a Tektronix 519 oscilloscope of combined resolution ~1 Gc. Under certain circumstances we observe a ~50 per cent modulation at the fundamental cavity frequency.

Stoicheff [2] has also shown that the spectral width of the anti-Stokes radiation in stimulated Raman scattering (SRS) is very sensitive to mode structure and that very narrow lines are to be expected with single longitudinal mode behavior. Such behavior has been observed in our laboratory and is shown in Figs. 2 and 3. This is perhaps our most sensitive test for single mode behavior.

It has been suggested [1], [5] that the conversion efficiency of GPL to Stokes radiation in SRS is also sensitive to the number of modes of the GPL and that the conversion efficiency for a single mode pump should be about an order of magnitude less. Measurements with our mode-controlled GPL, whose output consists of two TEM_{00n} modes spaced by 800 Mc (one of which was ~4 times stronger than the other) showed that this was not the case. On the contrary, the conversion efficiency at a given power density was precisely independent of the number of modes operating.

The transverse-mode structure was evaluated by observing the far-field pattern of the laser with a 1-m-focal length camera. The pattern observed with transverse-mode selection consisted of one lobe (TEM_{00}) or two lobes (TEM_{01}). The size of each lobe corresponded to the diffraction limit for the laser beam diameter. These patterns looked exactly like those observed by Evtuhov and Neeland [5] for single-transverse-mode operation in normal ruby lasers. The power output was ~2MW. Further details of transverse-mode selection will be published elsewhere.

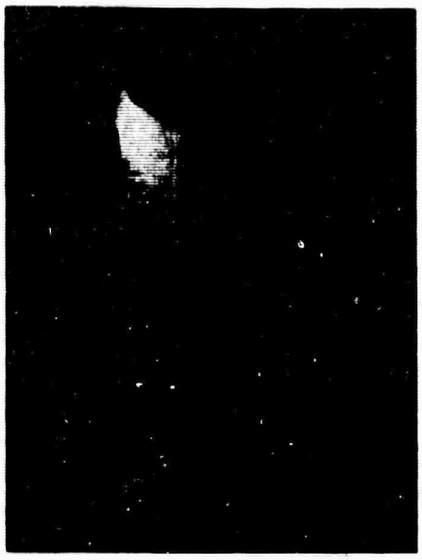

Fig. 2. First anti-Stokes stimulated Raman scattering in benzene showing a photograph of emission angle vs. wavelength without mode selection. The neon reference lines are separated by ~26 A. This distance corresponds to ~1.5° on the vertical scale. Neutral Density (N.D.) 1 filter covers half the slit. Copper shields were placed over the center of the slit where the laser was focused.

Fig. 3. First anti-Stokes stimulated Raman scattering in benzene showing a photograph of emission angle vs. wavelength with mode selection. The neon reference lines are separated by ~26 A. This distance corresponds to ~1.5° on the vertical scale. An N.D. 1 filter covers half the slit. Copper shields were placed over the center of the slit where the laser was focused.

Results

The results of the foregoing mode selection procedure can be seen in the various Fabry-Perot photographs of the laser output shown in Figs. 4–8. For Fig. 4, the 2.4-mm-spaced etalon is used, and for the others, the 20-mm-spaced etalon is used. In each picture a Neutral Density 0.6 filter covers about half the pattern.

Figure 4 shows the result of using the temperature tuning and the reflection mode selector only. The photograph shows an output consisting of two components separated by ~3 Gc. The spectral width here is limited by the 1-Gc resolution of the interferometer. When the temperature is raised by ~5°C, we observe two components of about equal intensity separated by 40 Gc. This separation corresponds to adjacent modes of the 2-mm-thick reflection mode selector. The laser output was 12 MW.

Figure 5 shows the result of adding our transmission mode selector to the foregoing configuration and adjusting its tilt for minimum laser linewidth. The laser output is ~5 MW. Careful examination of the photographic plate shows that ~80 per cent of the energy is in a single component ~450 Mc wide, which probably corresponds to two components of roughly equal intensity spaced by ~300 Mc. The rest of the energy is in four weak components that are spaced by ~1.2 Mc. We note that, because of halation and lack of dynamic range, such an output would appear to be a single longitudinal mode on polaroid film.

Figure 6 shows the effect of adding the cryptocyanine dye cell to the foregoing configuration while keeping the pumping level constant. The output is ~1 MW and appears as a single component ~300 Mc wide, which corresponds to a single longitudinal mode.

We have found the cryptocyanine dye insufficient by itself to suppress components 40 Gc apart when the laser output is ~10 MW. At these output levels the dye, usually but not reliably, suppresses some of the more closely spaced (~1 Gc) modes when used with the transmission mode selector. This effect is shown in Figs. 7 and 8, where the output is maintained at ~8 MW by pumping the laser harder when the dye is used. The configuration is somewhat different from that for Figs. 5 and 6 in that the distance between the reflection mode selector and the front of the ruby is changed from 12 cm to 18 cm and the total cavity length is changed from 50 cm to 70 cm. Figure 7 shows the laser output without the dye. There are one strong and four weak components, each ~300 Mc wide and spaced by ~800 Mc from the adjacent components. Figure 8 shows the effect of adding the dye. There are only two components ~300 Mc wide and of comparable intensity spaced by ~800 Mc. The 800-Mc splitting corresponds to the new ruby-to-reflector distance.

Finally, we note that another 3-in. × ¾-in. ruby gives essentially the same results as the one used previously.

Summary

It is possible to mode-select the rather broadband output of the ruby giant pulse laser without serious loss of power. The spectral purity of the output will depend to some extent upon the power output desired from the laser. In general, it appears possible to obtain as much as 80 per cent of the energy in a single longitudinal mode of the laser without sacrificing more than 30 per cent in the output power. A comparison of the observed line-

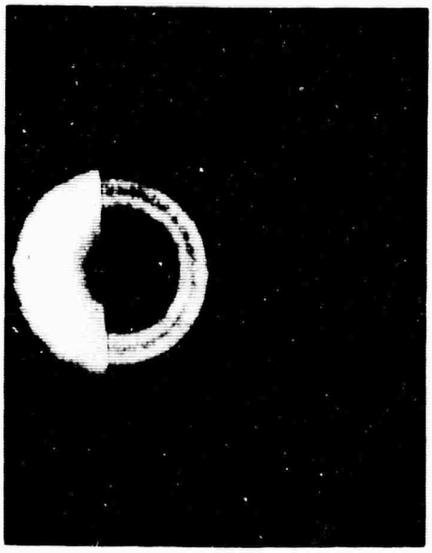

Fig. 4. Fabry-Perot pattern showing the effect of our reflection mode selector (RMS) when the ruby is temperature tuned to resonance.

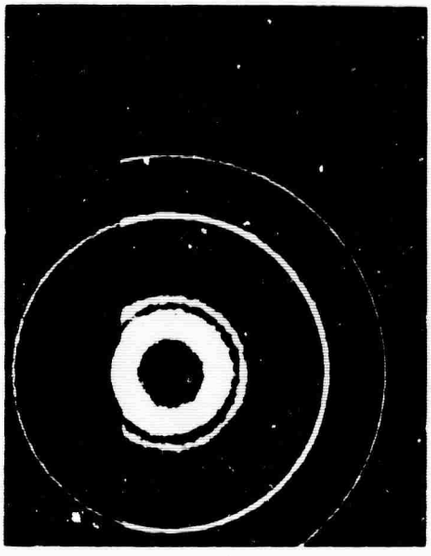

Fig. 5. Fabry-Perot pattern showing the effect of adding and tuning our transmission mode selector (TMS) to the RMS.

Fig. 6. Fabry-Perot pattern showing the effect of adding our cryptocyanine dye mode selector (CMS) to the TMS and RMS.

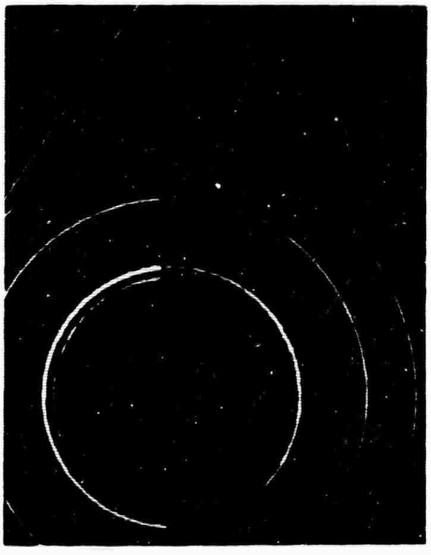

Fig. 7. Fabry-Perot pattern showing the effect of adding and tuning our TMS to the RMS.

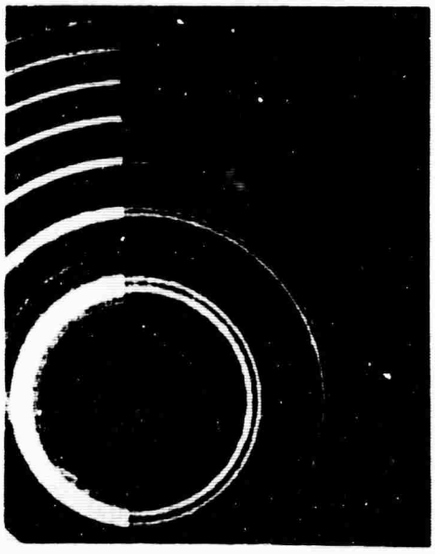

Fig. 8. Fabry-Perot pattern showing the effect of adding our CMS to the TMS and RMS.

width for the ruby laser with the instrument resolution indicates that the corrected ruby linewidth is about 200 Mc. This linewidth is considerably greater than the approximately 10-Mc transform from the pulse width measurements. This problem has not been reconciled, and possibly future work will aid in our understanding. Some possible explanations could be the frequency spreading associated with the presence of a large number of transverse modes, each having a slightly different frequency or weak components separated from the main one by the 200-Mc-mode interval of the laser. Also, there probably are independent regions with slightly different path lengths giving rise to slight frequency spread. Both of these hypotheses are consistent with our initial observations with a transverse-mode-controlled laser. Here the line-width of individual modes appears instrument-limited, but selected portions of the ruby are used for laser action.

ACKNOWLEDGMENTS

We wish to thank V. Evtuhov, J. K. Neeland, W. G. Wagner, and H. Winston for many illuminating discussions.

REFERENCES

[1] Bloembergen, N., and Y. R. Shen, Multimode effects in stimulated raman emission, *Phys. Rev. Letters*, vol 13, Dec 1964, pp 720–724.
[2] Stoicheff, B. P., Characteristics of stimulated raman radiation generated by coherent light, *Phys. Letters*, vol 7, Nov 1963, pp 186–188.
[3] Wagner, W. G., private communication.
[4] Soffer, B. H., Giant pulse laser operation by a passive, reversibly bleachable absorber, *J. Appl. Phys.*, vol 35, Aug 1964, p 2551.
[5] Weiner, D., S. E. Schwarz, and F. J. McClung, Comparison of observed and predicted stimulated raman conversion efficiencies, submitted to *J. Appl. Phys.*
[6] Evtuhov, V., and J. K. Neeland, Observations relating to the transverse and longitudinal modes of a ruby laser, *Appl. Optics*, vol 1, Jul 1962, pp 517–520.

Appendix II

MODE-STRUCTURE INDEPENDENCE OF STIMULATED RAMAN-SCATTERING CONVERSION EFFICIENCIES*

F. J. McClung, W. G. Wagner, and D. Weiner†

Hughes Research Laboratories, Malibu, California

(Received 13 April 1965)

The power density needed to convert a given amount of laser energy to stimulated Raman-scattered radiation has been found to be about an order of magnitude less in nitrobenzene than theoretically expected for the case of a Raman cell external to the laser cavity.[1] It has been suggested[1,2] that the multimode character of the laser pump might be responsible for this disagreement. Bloembergen and Shen[2] have given a semiquantitative estimate of the enhancement of the Raman gain. It indicates that with a typical multimode laser a Raman gain ~4 to 8 times greater than that for a single-mode laser should be produced. It is the purpose of this communication to show that the Raman gain in nitrobenzene for a single-mode laser pump is precisely that for a multimode laser pump, and to suggest other reasons for the above-mentioned disagreement.

In this experiment, the collimated beam from our giant pulse laser was directed onto a 1.45-mm aperture 70 cm from the laser, and the portion of the beam transmitted by the aperture passed through a 10-cm cell of nitrobenzene onto a MgO diffuse reflector placed 50 cm after the cell. The power of the laser and the first Stokes line was monitored by suitably filtered fast photodetectors that sampled the diffuse reflection from the MgO. The cell was tilted at ~3° with respect to the laser beam. This arrangement is like that described in more detail by Weiner, Schwarz, and McClung,[1] except that the aperture and cell are now further from the laser and closer to the MgO. Also, another beam splitter to allow a measurement of the far-field pattern has been added.

Our laser has been mode-selected to give single-transverse and longitudinal mode behavior. The details of the mode-selection techniques will be given elsewhere.[3] The transverse mode structure was determined with the aid of a 1-m focal-length camera. The longitudinal mode structure was determined with the aid of a 2-cm spaced Fabry-Perot etalon with $\lambda/80$ flat plates of ~1% transmission. When completely mode-selected, the laser produced 2 MW of power in a beam whose divergence equaled the diffraction limit corresponding to the laser-beam diameter. When not mode-selected, the laser output was ~10 MW, the beam divergence $\sim 1.5\times10^{-3}$ rad, and the spectral width $\sim\frac{1}{2}$ cm^{-1}. The pulse length was ~30 nsec for both cases. The results of the conversion-efficiency measurements for mode-selected and non-mode-selected lasers are shown in Table I. The experimental arrangement is the same for both cases. The relative error for the power measurements is ~5%. Measurements at other power densities for our mode-selected laser gave a conversion-efficiency curve which agreed very well with our previous curve for a non-mode-selected case.[1] The data of Table I indicate strongly that the anomalously high gain is not caused by the laser mode structure.

The theoretical gain in nitrobenzene at 20 MW/cm is 0.028 cm^{-1}. This gain is computed using a formula of Hellwarth[4] and a recently measured peak Raman-scattering cross section of 1.3 ± 0.4 cm^{-2}. This cross section agrees within the expected error with our earlier[5] and less accurate measurement of 2.3 ± 1.2 cm^{-1}. It also agrees with the recent measurement of Damen, Leite, and Porto[6] in the fol-

Table I. Conversion efficiency for mode-selected and non-mode-selected pumping of nitrobenzene.

Description of mode structure	Incident-peak power density (MW/cm^2)	Power converted to first Stokes radiation (%)
Two TEM_{00} modes of ~4:1 intensity ratio separated by ~800 Mc/sec	19	0.6
~100 transverse modes ~10-20 longitudinal modes	19.5	0.6

lowing sense. If we scale our data for benzene cross sections by the ratio of the nitrobenzene cross sections (1.3/2.3) and then compute the cross section/molecule at 6328 Å, we find a value of $0.7 \pm 0.2 \times 10^{-29}$ cm^2. Here we assume a λ^4 wavelength dependence and use the observed angular dependence for Raman scattering. This value agrees (within the stated error) with their[6] value of $0.56 \pm 0.1 \times 10^{-29}$ cm^2.

To estimate the Raman gain at 20 MW/cm^2 from our conversion-efficiency data, we assume noise is amplified during a double pass (through the cell to the laser reflectors and back through the cell) to the observed level of 10^8 W/cm^2. The dominant contribution to the noise which initiates the generation of the Raman-shifted radiation comes from the quantum-mechanical zero-point vibrations of the electromagnetic field. In a spectral interval of $d\lambda$, and within a cone of opening angle θ, centered on the axis of the laser beam, there is a zero-point power flux[7] given by $(\pi\theta^2\hbar\omega/n\lambda^3)(d\lambda/\lambda)$. Our measurements indicate that the bulk of the Stokes radiation emerges within an angle, θ, which is not greater than 0.017 rad, and that the fractional wavelength spread, $d\lambda/\lambda$, is of order 3×10^{-4}, and thus the starting power flux is estimated to be $< 1.2 \times 10^{-2}$ W/cm^2. Then 10^8 $W/cm^2 = 1.2 \times 10^{-2}$ $W/cm^2 \times \exp(g \times 20$ cm), so that the gain per cm $g = 0.80$ cm^{-1}. The gain is only slightly lower if calculated for multiple double passes where the feedback is supplied by diffuse reflection from the cell window and the MgO reflector, since the solid angle of acceptance imposed by our geometry is so small. Thus the observed gain is at least 25 times greater than that calculated from the cross sections.

We are very grateful for the penetrating, stimulating, and helpful comments of Dr. Shaul Yatsiv during the course of this work.

---

*This work was partially supported by the Electronic Technology Division, Avionics Laboratory, Research and Technology Division, U. S. Air Force Systems Command, Wright-Patterson Air Force Base, Ohio, under Contract No. AF33(657)-11650.

†Present address: Department of Electrical Engineering, University of California, Berkeley, California.

[1]L. Weiner, S. E. Schwarz, and F. J. McClung, to be published.

[2]N. Bloembergen and Y. R. Shen, Phys. Rev. Letters 13, 720 (1964).

[3]F. J. McClung and D. Weiner, to be published.

[4]R. W. Hellwarth, Appl. Opt. 2, 847 (1963).

[5]F. J. McClung and D. Weiner, J. Opt. Soc. Am. 54, 641 (1964).

[6]T. C. Damen, R. C. C. Leite, and S. P. S. Porto Phys. Rev. Letters 14, 9 (1965).

[7]It is assumed that the Raman radiation is strongly polarized, in accord with the experiments. The wavelength to be used in the formula is that of the Stokes radiation, inside the Raman cell, and n is the linear index of refraction at the Stokes frequency ω.

APPENDIX III

The Self-Focusing of Light of Different Polarizations[†]

D. H. Close, C. R. Giuliano, R. W. Hellwarth,
L. D. Hess, F. J. McClung, and W. G. Wagner

Hughes Research Laboratories, Malibu, California

Abstract — In an effort to verify the hypothesis that molecular reorientation (ac Kerr effect) is responsible for the self-focusing of light beams in certain liquids, we have measured and compared the thresholds and other characteristics of self-focusing for circularly and linearly polarized beams incident on these liquids. We show that for plane waves propagating in a homogeneous, isotropic, ensemble of molecules having anisotropic polarizability tensors, the non-linear index should be four times as great for linearly as for circularly polarized waves. The hope that this difference in indices would be reflected in a four fold increase in the threshold power for self-trapping when circularly instead of linearly polarized light is incident was not realized. In practice, the increase was always found to be much less. However, in every case studied, the trapped light from a beam, circularly polarized to better than one part in 200, was markedly, if not completely, depolarized as soon as self-trapping could be detected.

[†] This work has been supported in part as a part of Project DEFENDER under the joint sponsorship of the Advanced Research Projects Agency, the Office of Naval Research, and the Department of Defense.

We show qualitatively when this polarization instability should exist for all but linearly polarized light and for a variety of nonlinear mechanisms. However, in the absence of even an approximate quantitative theory of the self-trapping of light that is not linearly polarized, the comparative measurements of thresholds cannot be said either to verify or disprove the hypothesis of molecular reorientation.

I. INTRODUCTION

Self-focusing and trapping of high power electromagnetic beams was foreseen by Askar'yan,[1] Talanov,[2] and Chiao, Garmire, and Townes,[3] and has now been observed in many liquids.[4-8] In this effect the third order nonlinear index of refraction of a substance causes the incident light beam to focus or "trap" itself into one or more narrow beams or "filaments." In their original discussion of self-focusing at optical frequencies, Chiao, et al.,[3] estimated the relative thresholds for self-trapping that might be expected from each of three physical mechanisms: molecular reorientation in the strong optical fields (ac Kerr effect), electrostriction, and the nonlinear electronic polarizability. Recent comparisons of these estimated thresholds with thresholds observed in liquids which readily exhibit stimulated Raman scattering have suggested that molecular reorientation is most likely the mechanism underlying the self-trapping (and hence also the anomalously low Raman and Brillouin thresholds) in these liquids.[5-7] In this paper we report the results of attempts to verify this molecular reorientation hypothesis by measuring the ratio of the thresholds for the self-trapping of a linearly polarized beam to the threshold for a circularly polarized beam. We have found an instability in the nonlinear propagation of circularly polarized light which has made interpretation of the threshold results difficult.

Both a linearly polarized plane wave and a circularly polarized plane wave are solutions of the nonlinear Maxwell equations for a spatially local nonlinear polarizability proportional to the field cubed. In general, a linearly polarized wave propagates with a different (nonlinear) index of refraction than a circularly polarized wave. If the

nonlinear index arises from molecular reorientation, it is a straightforward matter to show that the real nonlinear part of the index for linear polarization should be four times that for circular, regardless of the shape of the molecules being oriented. If one then supposes that at least the onset of trapping for each case can be dealt with by geometrical optics incorporating nonlinear indices, as has been done by Kelley,[9] the power required to begin trapping a circularly polarized beam should be four times that required to self-trap a linearly polarized beam.

Our experiments show that only between one and three times as much circularly polarized power is required in the many liquids we have examined. However, we have found that, although light trapped from a linearly polarized input beam emerges linearly polarized, light trapped from a circularly polarized input beam is largely, if not completely, depolarized as soon as we have been able to observe it. This fact we attribute to an instability in the propagation of circularly polarized light. We show that this instability may exist whenever the coefficient of the term $(\bar{E}_\omega \cdot \bar{E}_\omega)\bar{E}^*_\omega$ in the expansion of the polarization amplitude $\bar{P}_\omega$ is positive. ($\bar{E}_\omega$ is the amplitude of the electric field at frequency ω.) This coefficient has been called $B/2$ by Maker, et al., who measured it in a variety of liquids and found it always to be positive.[10] The coefficient B will be positive if molecular reorientation or electronic nonlinearities dominate and doubtless will be positive for many other possible physical mechanisms as well. We have not discovered any mechanism for which the coefficient should be negative (where no other frequencies are present in strength), but it should be zero for stationary electrostriction. The fact that thresholds for trapping do not agree with the simple predictions of molecular reorientation does not rule out molecular orientation as the main mechanism because the nonlinear propagation of circularly polarized light appears to be incorrectly treated by all the techniques devised to date. Only the nonlinear index for linearly polarized light can be obtained from

trapping measurements in liquids studied to date, for a linear state of polarization is the only state which propagates in a manner which can be approximated by the scalar nonlinear equations studied so far.

II. THEORY

AC Kerr Effect

In the present experiments we are interested in situations where the thermal energy kT is much larger than a rotational quantum of energy, which is in turn much larger than the interaction energy of a molecule with the strong electric fields. We are therefore led to describe the molecules in the liquids classically. The probability $P(\Omega)$ for a molecule to have its major dielectric axes oriented at the Euler angles θ, ϕ, ψ (symbolized by Ω) is given by

$$P(\Omega) = \frac{\exp\left[-U(\Omega)/kT\right]}{\int d\Omega \exp\left[-U(\Omega)/kT\right]} \qquad (1)$$

where the energy $U(\Omega)$ of a molecule interacting with the field is given by

$$U(\Omega) = -\frac{1}{2} \Sigma_{i,j} \overline{F_i(t)\, F_j(t)}\ a_{ij}(\Omega) \ , \qquad (2)$$

the bar indicating a time average over many cycles of the local optical electric field $F_i(t)$. The indices i, j represent the spatial indices x, y, z. Here $a_{ij}(\Omega)$ is the polarizability tensor for a molecule oriented at the angles Ω. When the principal axes of the dielectric ellipsoid are oriented along the x, y, z axes, then a_{ij} is diagonal, its three elements having the values $a, b,$ and c.

In order to compute the desired nonlinear dielectric constant, we need only the statistical average $\langle a_{ij} \rangle$ of a_{ij} over angles Ω to second order in the fields $F_i(t)$. It is a straightforward matter to perform the averaging with the weight function (1) and obtain

$$\langle a_{ij} \rangle = a\,\delta_{ij} + \gamma_{ij} \tag{3}$$

where $a = (a + b + c)/3$ is the usual linear optical polarizability of a molecule and

$$\gamma_{ij} = \left[\frac{(a-b)^2 + (b-c)^2 + (a-c)^2}{90\,kT}\right] \Sigma_{k,\ell}\,(3\delta_{ik}\,\delta_{j\ell} - \delta_{ij}\,\delta_{k\ell})\,\overline{F_k(t)F_\ell(t)} \tag{4}$$

is the nonlinear part of the polarizability. Although for a single plane wave only the parts of γ_{ij} having $i, j = x, y$ are needed, for a general treatment of trapping all space components of γ_{ij} would be needed. We may take the local field $F_i(t)$ to be related to the macroscopic electric field $E_i(t)$ by the linear Lorentz-Lorenz formula, provided that the nonlinear change in index is small. Then, if ρ is the number density of molecules,

$$F_i(t) = E_i(t)/(1 - 4\pi a\rho/3)\ . \tag{5}$$

Following further application of the Lorentz-Lorenz local field approximation, the polarizability tensor of (4) predicts that, for a linearly polarized plane wave of peak amplitude E_o, the linear index of refraction n is altered by an increment Δn_ℓ given by

$$\Delta n_\ell = \left(\frac{(a-b)^2 + (b-c)^2 + (c-a)^2}{45\,n\,kT}\right)\left(\frac{n^2+2}{3}\right)^4 \pi\rho E_o^2\ . \tag{6}$$

For a circularly polarized plane wave, (4) leads to an increment Δn_c to the linear index n which is related to the increment in (6) by

$$\Delta n_c = \Delta n_\ell/4\ . \tag{7}$$

Many other relations are contained in the expression (4) for the nonlinear polarizability including the usual expression for the ac and dc Kerr constants (the latter for nonpolar molecules only) which follow from the relation of Langevin between the change in index Δn_{ℓ} for light polarized parallel to a strong linearly polarized field and that $\Delta n_{\perp}$ for light polarized perpendicular to it:

$$\Delta n_{\perp} = - \Delta n_{\ell}/2 \ . \tag{8}$$

Stability of Polarization in Trapping

If an electric field having space components of the form $\mathrm{Re}\ E_i(\underset{\sim}{r})e^{-i\omega t}$ exists in an isotropic homogeneous medium with which it interacts locally in space, then the i^{th} spatial component of the polarization density may be written $\mathrm{Re}\ P_i(\underset{\sim}{r})e^{-i\omega t}$ where

$$P_i = \chi_j E_j + \chi_{ijk\ell}\ E_j E_k E_{\ell}^{*} \tag{9}$$

to third order in the fields. From the isotropy of the medium, it follows that we may write

$$\chi_{ijk\ell} = A\ \delta_{ij}\delta_{k\ell} + \frac{1}{2}\ B\ \delta_{i\ell}\delta_{jk} \tag{10}$$

where we have followed the nomenclature of Maker, et al.[10] In a lossless medium with a nonlinear susceptibility of the form (10), Maxwell's equations are satisfied by (among many other things) two parallel circularly polarized plane waves propagating with indices altered by increments

$$\delta n_{\pm} = (2\pi/n)\left[A\ E_{\pm}E_{\pm}^{*} + (A + B)\ E_{\mp}E_{\mp}^{*}\right] \tag{11}$$

respectively for the right and left circularly polarized waves of amplitudes $E_{\pm} \equiv (E_x \pm i E_y)/\sqrt{2}$. However, the propagation of a monochromatic, finite size, diffraction limited parallel beam cannot be simply described by several indices as in (11). Nevertheless, we can guess what might happen to such a finite beam, launched in an arbitrary state of polarization from a plane at $z = 0$, by a study of (11). For some region of $z > 0$ one expects that the circular components will essentially just have their phase relations altered according to the difference in indices predicted by (11). That is, the major axis of the initial polarization ellipse will be rotated by an angle proportional to Bz.† However, beyond a certain distance z_o, the fact that the radial index change (caused by the variation in intensity across the beam) is different for one circular component than for the other (unless $|E_+| = |E_-|$) suggests that one component will be self-focused more strongly than the other, and hence the polarization in the trapped parts of the beam will change with length.

If A and B are positive (which seems to be the case in all materials studied so far and which holds for the a Kerr effect), then the weaker of the two circular components is seen to be self-trapped before the stronger because of its greater increase in index. It is this tendency of the weaker cirulcar component to increase in intensity that we believe underlies the observed depolarization of the filaments formed from a nearly circularly polarized beam. A perfectly circularly polarized incident beam is impossible to obtain and hence any nominally circularly polarized beam can be expected to degenerate into randomly oriented linearly polarized filaments. If the incident beam is linearly

† It was by measuring the rotation of the polarization ellipse that Maker, et al., originally attempted to measure the B coefficients for various materials.[10]

polarized, then any slight deviation of equality between E_+ and E_- will tend to trap the weaker component and restore the perfectly linear polarization. Hence, only linearly polarized light can be thought of as a single stable propagating component and be treated approximately with scalar nonlinear equations. It is to be emphasized that no approximate quantitative treatment of the self-focusing of other than a linearly polarized beam has been put forth as yet, and the arguments presented above on the basis of (11) are qualitative at best.

We note from (4) that one may easily conclude that $B/A = 6$ for the ac Kerr effect. For a nonlinear electronic polarizability it is easy to show that $A = B$; and for static electrostriction that $B = 0$. A weak left handed component in the presence of a strong right handed one is focused at a power $(2A + B)/2(A + B)$ times the threshold to trap linearly polarized beam.[3,†]

† The birefringence induced in a weak beam of light at 5000 Å by a strong linearly polarized beam at 6943 Å has been measured in several liquids by Guy Mayer and Francois Gires in "Action d'une onde lumineuse intense sur l'indice de réfraction des liquids," Comptes Rendus, Vol. 258, pp. 2039-2042, February 1964. The coefficient which they used to describe their results (and called B_o in analogy with the dc Kerr coefficient), is, in general, independent of the coefficients A and B discussed above, as B_o describes the effect of two frequencies separated by more than the thermal relaxation rates. However, if molecular reorientation were entirely responsible for the induced birefringence and self-trapping, and if the two frequencies in the former are not too far apart, it is easy to deduce from our eq. (4) that the B_o and B would be related by $B = n\lambda B_o/4\pi$ where λ is the free space wavelength of the weak birefringent beam. Using this relation to deduce values for B from the measurements of B_o by Mayer and Gires gives values roughly an order of magnitude higher than those obtained in Ref. 10. However, Wang and Racette have recently remeasured B using unfocused rather than focused beams and reported (at the 1966 International Quantum Electronics Conference) much higher values than were reported in Ref. 10. Using these new B values and some refined measurements of B_o reported by Mayer at the same conference, we calculate the ratio $R \equiv n\lambda B_o/(4\pi B)$ to be 1.3, 1.3, 1.9, and 1.9, respectively, for CS_2, nitrobenzene, toluene, and benzene. These remaining deviations of R from unity cast some doubt on the molecular reorientation hypothesis, but may still be the result of experimental uncertainties.

III. EXPERIMENTAL RESULTS

We have measured the relative thresholds for self-trapping of linearly and circularly polarized light in a number of liquids by two methods. The first method was to measure photometrically the thresholds for stimulated Raman scattering. This gives a fairly accurate measure for the trapping thresholds in those liquids which show strong self-focusing and Raman effect; the thresholds for the appearance of both then coincide.[5] The second method is to look photographically for the first appearance of self-focusing in the time averaged beam profile at the exit face of the liquid under study. In both types of experiments linearly polarized light was found to produce like-polarized filaments and Stokes output, whereas circularly polarized light produced depolarized filaments and Stokes output.

Photometric Measurements

For the photometric measurements, the unfocused beam of a ruby laser was first passed through crossed Glan polarizers which served as a variable attenuator and supplied a purely linearly polarized output beam. The unfocused beam then passed through a 10 cm cell containing the liquid in which self-trapping was to be studied. A portion of the output beam from this cell was split off and monitored by silicon photodiodes for Stokes energy content after passing through a Corning 5-56 filter, two Wratten 89B filters, and appropriate attenuators. When the liquid cell was removed, the laser produced no signal at the photodetector, thus assuring that only Stokes light was being measured.

Typical results for the Stokes output powers plotted as a function of either linearly or circularly polarized inputs are given for benzene, nitrobenzene, and CS_2 in Fig. 1. From such data the trapping threshold ratios (linear to circular) for various liquids is given in Table I. These ratios are seen to be consistently well below the value 4 expected if circularly polarized light would produce circularly polarized filaments via the ac Kerr effect.

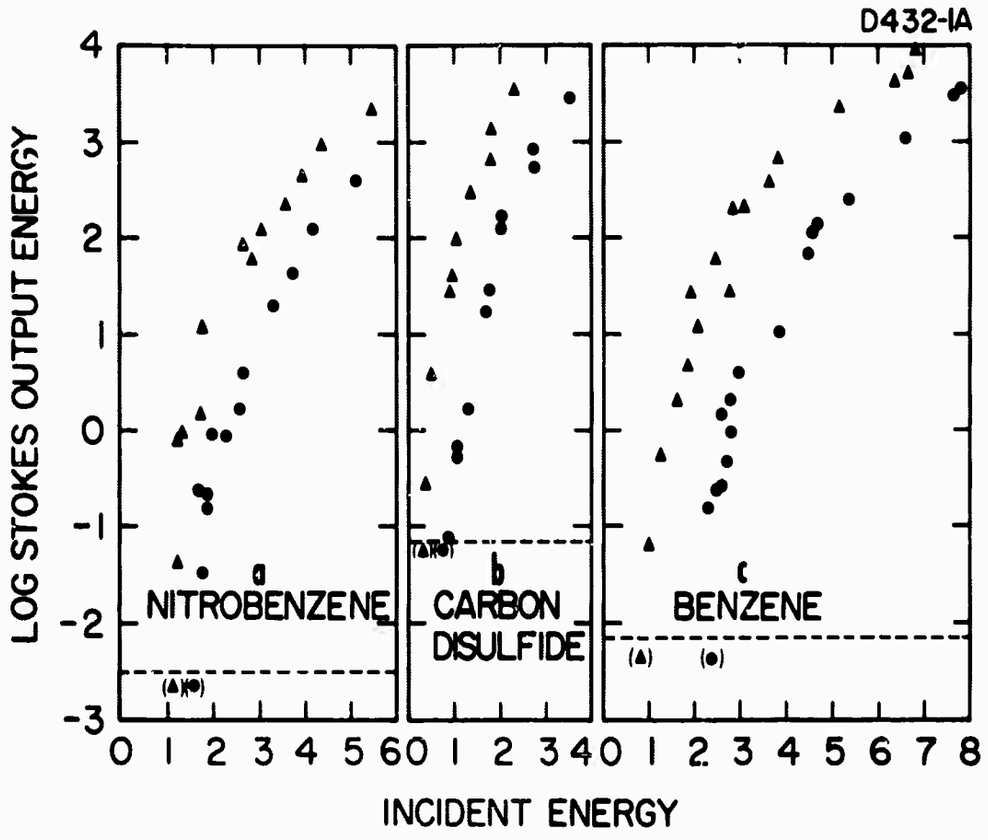

Fig. 1. Plots of the Raman Stokes output energy versus ruby laser energy incident on a 10 cm cell of (a) nitrobenzene, (b) carbon disulphide, and (c) benzene. Triangular points represent linearly polarized incident light, circular points represent circularly polarized light. The zero of the log Stokes output energy corresponds roughly to a conversion of 10^{-5} of the laser energy to Stokes energy. The incident energy was not calibrated absolutely. The dotted lines represent pulses producing no detectable Stokes output.

TABLE I

Ratios of Incident Light Powers Required to Reach Threshold for Stimulated Raman Scattering (hence self-focusing) in Various Liquids

Liquid	Threshold Ratio Circular:Linear
Nitrobenzene	1.4(2)[a]
Carbon Disulfide	2.0(3)
Benzene	2.2(7)
Bromobenzene	1.7(5)
Toluene	1.2(3)
Benzoyl Chloride	1.3(4)
Acetone	1.3(5)

[a]The figures in parentheses give the uncertainty in the last figure estimated from the scatter of data points.

The depolarization of the Stokes Raman output from nitrobenzene was also studied photometrically by imaging the exit window of the cell through a Fresnel rhomb and a Wollaston prism so as to form two images on a boron nitride surface. The images were monitored separately by silicon photodiodes through filters. Depending on the relative orientation of the Wollaston prism to the Fresnel rhomb, signals produced by the two images were proportional either to the right and left circular component intensities or to the intensities of the components linearly polarized parallel and perpendicular to the original laser polarization. When the cell was removed, the signals showed that only the nominal input polarization (either linear or circular) was present to within one part in 200, the limit of resolution. When Stokes light was produced by linearly polarized

input, it was found to be linearly polarized to within one part in 200; when it was produced by a circularly polarized input, it was found to contain equal intensities of both circular polarizations and of both linear polarizations. These results applied over the entire power range where Stokes light could be observed (rougly seven orders of magnitude variation in Stokes output). Also, apertures, from 1/2 to 5 mm diameter, placed in the laser beam did not affect these findings, even when the cell containing the liquid was placed in the far field of the 1/2 mm aperture.

Photographic Techniques

In the photographic measurements, the output from a ruby laser was passed through attenuating filters, a 1.5 mm diameter aperture and a rotatable quarter wave plate into a 10 cm cell containing the liquid under study. The output end of the cell was imaged through a Fresnel rhomb and Wollaston prism onto the entrance aperture of a low-dispersion grating spectrograph. The output of the spectrograph was recorded on Eastman Kodak 1N spectroscopic plates. A single laser pulse then produced six (or eight) separate images magnified about eight times and representing two orthogonal polarization components of the incident laser beam and the first and second (and, in the case of CS_2, the third) Stokes shifted output beams. The Stokes orders all appeared in filaments which were of the order of 5 to 30 μ in diameter, several times smaller than the corresponding filaments ($\sim$30 - 50 μ diameter) in the laser beam. The first Stokes filaments were of the same order of intensity as the laser beam filaments.

If the input beam was linearly polarized, the filaments and Stokes outputs from nitrobenzene and CS_2 were like-polarized to within one part in 10^3, the limit of instrumental resolution. However, if the input beam was circularly polarized, then the filaments and Stokes outputs from nitrobenzene contained equal amounts of both circular polarizations over the entire range of observability ($\sim$ three orders of magnitude

in the first Stokes intensity). The right and left circularly polarized images at any one output frequency were identical in every detail. When the Wollaston prism was rotated to test for orthogonal linearly polarized components under the same (circular) input conditions, the total intensity of one polarization in all of the filaments at a given frequency was equal to the total filament intensity of the orthogonal polarization, in agreement with the results of the photometric studies. However, the filament pattern for one linear component and frequency did not now agree in detail with the pattern for the orthogonal polarization (at the same frequency) but suggested that each filament might consist mainly of light linearly polarized in some random direction.

The photographic comparison of circular and linear thresholds was more difficult and less accurate than the photometric comparisons. A plot of the number of Stokes filaments observed as a function of both linearly and circularly polarized input energies indicated that the threshold ratios were less than four, but perhaps somewhat higher than those in Table I for CS_2 and nitrobenzene.

Similar experiments with circularly polarized light trapped in CS_2 showed some slightly different results. There was incomplete depolarization, only of order of one third of the filament energy appearing in the oppositely polarized laser and first Stokes filaments. However, the partition of energy was more nearly equal in the second Stokes output and became essentially equal in the third Stokes output.

In the above and previous photographic studies,[6] in which the output light is averaged over the entire ($\sim$25 nsec) duration of the laser pulse, trapped filaments appeared to be at most twice as intense as the average beam intensity, and hence the explanation of the observed Raman gains (several orders of magnitude larger than predicted) was not complete. To clarify further the role of trapping in producing anomalous Raman gains, we made time-resolved photographs looking through the spectrograph at the exit end of the cell (but with the Fresnel rhomb and Wollaston prism removed). These showed, as expected, that at their

peak intensity, trapped fialments were one to two orders of magnitude brighter than the background. The laser filaments appeared at different times lasting typically 3-6 nsec. The first Stokes fialments were observed to persist for a shorter duration, ~1 to 2 nsec. These observations showed qualitative agreement between the expected Raman gain and the laser intensity.

REFERENCES

1. G. A. Askar'yan, Zh. Experim. i Theor. Fiz., vol. 42, pp. 1567-1570, Translation: "Effects of the gradient of a strong electromagnetic beam," Soviet Phys. — JETP, vol. 15, pp. 1088-1090; December 1962.

2. V. I. Talanov, "On self-focusing of electromagnetic waves in non-linear media," Izvestia Vysshikh Uchebnykh Zavedenii. Radiofizika, vol. VII, pp. 564-565, Issue 3, 1964.

3. R. Y. Chiao, E. Garmire, and C. H. Townes, "Self-trapping of optical beams," Phys. Rev. Letters, vol. 13, pp. 479-482; October 1964.

4. N. F. Pilipetskii and A. R. Rustamov, "Observation of self-focusing of light in liquids," Soviet Phys. — JETP Letters, vol. 2, pp. 55-56; July 1965.

5. Y. R. Shen and Y. J. Shaham, "Beam deterioration and stimulated Raman effect," Phys. Rev. Letters, vol. 15, pp. 1008-1010; December 1965.

6. P. Lallemand and N. Bloembergen, "Self-focusing of laser beams and stimulated Raman gain in liquids," Phys. Rev. Letters, vol. 15, pp. 1010-1012; December 1965.

7. C. C. Wang, "Length-dependent threshold for stimulated Raman effect and self-focusing of laser beams in liquids," Phys. Rev. Letters, vol. 16, pp. 344-346; February 1966.

8. E. Garmire, R. Y. Chiao, and C. H. Townes, "Dynamics and characteristics of the self-trapping of intense light beams," Phys. Rev. Letters, vol. 16, pp. 347-349; February 1966.

9. P. L. Kelley, "Self-focusing of optical beams," Phys. Rev. Letters, vol. 15, pp. 1005-1008; December 1965.

10. P. D. Maker, R. W. Terhune, and C. M. Savage, "Intensity-dependent changes in the refractive index of liquids," Phys. Rev. Letters, vol. 12, pp. 507-509; May 1964.

BLANK PAGE

APPENDIX IV

Details of a Calculation of the Term U_{22} in the Fourth Order Electric Free Energy

Here we outline the calculation of $U_{22} = \langle\langle u_2^2 \rangle\rangle - \langle\langle u_2 \rangle\rangle^2$. We will use the form of eq. (37)* for the probability $V^{-2}\, p(\underline{r}_1 - \underline{r}_2)\, d^3\underline{r}_2 d^3\underline{r}_2$ that if a certain molecule is in $d^3\underline{r}_2$, another specified molecule is in $d^3\underline{r}_2$. We will use Kirkwood's superposition approximation for $V^{-3}\, p_3(\underline{r}_1, \underline{r}_2, \underline{r}_3) \equiv p_3(123)$ [and for $V^{-4}\, p_4(\underline{r}_1, \underline{r}_2, \underline{r}_3, \underline{r}_4) \equiv p_4(1234)$] which is the probability (per unit volume for each molecule) for finding specified molecules at $\underline{r}_1$, $\underline{r}_2$, $\underline{r}_3$ (and $\underline{r}_4$) simultaneously:

$$p_3(123) \approx p(12)\, p(23)\, p(13) \tag{A1}$$

$$p_4(1234) \approx p(12)\, p(13)\, p(14)\, p(23)\, p(24)\, p(34) \ . \tag{A2}$$

Here $p(12)$ is an abbreviation for $p(\underline{r}_{12})$, and we have ignored terms of order N^{-2} smaller than the leading terms of (A1) and (A2). (Terms of order N^{-1} must be kept, as the terms in U_{22} which are proportional to N^2 will cancel.)

The integrals in $4 \langle\langle u_2^2 \rangle\rangle$ fall naturally into four groups, which we call I_1, I_2, I_3, and I_4, depending on whether 1-, 2-, 3-, or 4-particle correlations are required:

$$4 \langle\langle u_2^2 \rangle\rangle = \sum_{i=1}^{4} I_i \tag{A3}$$

where

$$I_1 = \sum_{\mu} \langle\langle (\underline{E}' \cdot \underline{\underline{a}}^{\mu} \cdot \underline{\underline{D}}^{\mu\mu} \cdot \underline{\underline{a}} \cdot \underline{E}')^2 \rangle\rangle = 0 \tag{A4}$$

---

*Equation numbers in text refer to those in the main body of the report.

$$I_2 = 2\Sigma_{\mu\nu} << (\underset{\sim}{E}' \cdot \underset{\sim}{a}^{\mu} \cdot \underset{\sim}{D}^{\mu\nu} \cdot \underset{\sim}{a}^{\nu} \cdot \underset{\sim}{E}')^2 >> \tag{A5}$$

$$I_3 = 4\Sigma_{\mu\nu\gamma} << \underset{\sim}{E}' \cdot \underset{\sim}{a}^{\mu} \cdot \underset{\sim}{D}^{\mu\nu} \cdot \underset{\sim}{a}^{\nu} \cdot \underset{\sim}{E}'$$

$$\underset{\sim}{E}' \cdot \underset{\sim}{a}^{\nu} \cdot \underset{\sim}{D}^{\nu\gamma} \cdot \underset{\sim}{a}^{\gamma} \cdot \underset{\sim}{E}' >> \tag{A6}$$

and

$$I_4 = \Sigma_{\mu\nu\beta\gamma} << \underset{\sim}{E}' \cdot \underset{\sim}{a}^{\mu} \cdot \underset{\sim}{D}^{\mu\nu} \cdot \underset{\sim}{a}^{\nu} \cdot \underset{\sim}{E}'$$

$$\underset{\sim}{E}' \cdot \underset{\sim}{a}^{\beta} \cdot \underset{\sim}{D}^{\beta\gamma} \cdot \underset{\sim}{a}^{\gamma} \cdot \underset{\sim}{E}' >> . \tag{A7}$$

Here the summed indices are always unequal in any I_i. The I_1 is zero of course because $\underset{\sim}{D}^{\mu\mu}$ is defined to be zero. The angular averages in each of the remaining integrals are easily performed and give

$$I_2 = 2a^4 E'^4 \Sigma_{\mu\nu} \left[(1 + \Delta^2/4)^2 < (D_{xx}^{\mu\nu})^2 > + (\Delta^2/2 + 11\,\Delta^4/16) < \mathrm{Tr}\, \underset{\sim}{D}^{\mu\nu} \cdot \underset{\sim}{D}^{\mu\nu} > \right] \tag{A8}$$

$$I_3 = 4a^4 E'^4 (1 + \Delta^2)\, \Sigma_{\mu\nu\gamma} < D_{xx}^{\mu\nu} D_{xx}^{\nu\gamma} > \tag{A9}$$

$$I_4 = a^4 E'^4 \Sigma_{\mu\nu\beta\gamma} < D_{xx}^{\mu\nu} D_{xx}^{\beta\gamma} > \tag{A10}$$

Here "Tr" denotes the "trace" or sum over diagonal space elements, and the single bracket $<>$ denotes the average over spatial configurations.

Using the form (37) for the two particle distribution function and (20) for $D^{\mu\nu}$ gives (neglecting terms $\sim 1/N$)

$$\Sigma_{\mu\nu} < (D_{xx}^{\mu\nu})^2 > = N^2 V^{-1} 4\pi \int_0^{\pi} \sin\psi\, d\psi \int_0^{\infty} r^2\, dr (1 - 3\cos^2\psi)^2 r^{-6}$$

$$= N\rho\, 64\, \pi^2/(45\, \tau) \, . \tag{A11}$$

Similarly,

$$\Sigma_{\mu\nu} \langle \mathrm{Tr}\, \underline{D}^{\mu\nu} \cdot \underline{D}^{\mu\nu} \rangle = N^2 V^{-1}\, 12\pi \int_0^{\pi} \sin\psi\, d\psi \int_d^{\infty} r^2\, dr$$

$$\cdot\, (1 + 3\cos^2\psi) r^{-6} = N\rho\, 32\, \pi^2/(3\tau) \quad . \tag{A12}$$

Therefore,

$$I_2 = N a^4 E'^4\, \rho^2\, 4\, \pi^2 (32 + 136\, \Delta^2 + 167\, \Delta^4)/(45\, \rho\tau) \quad . \tag{A13}$$

To perform the average in (A9) to order N, we write

$$p(r) = (1 - h(r))/(1 - \tau/V) \tag{A14}$$

where $h(r) = 1$ for $r < d$ and is zero otherwise. Then, with (A1), we obtain to order N

$$\Sigma_{\mu\nu\gamma} \langle D^{\mu\nu}_{xx}\, D^{\nu\gamma}_{xx} \rangle = N^3 V^{-2} \int d^3 \underline{r}_2\, d^3 \underline{r}_3\, \bar{D}_{12}\, \bar{D}_{23}\, (1 - h_{13}) \quad , \tag{A15}$$

where $\bar{D}_{12} \equiv D^{12}_{xx}(1 - h_{12})$, h_{12} denotes $h(\underline{r}_2 - \underline{r}_3)$, etc. The integrals here are easily performed using the theorem that the integral J of $\bar{D}_{12}$ over any volume Q is related to an integral over the surface S bounding Q by

$$J = \int_Q d^3 \underline{r}_2\, \bar{D}_{12} = - \int_S d^2 \underline{r}_2\, \hat{n} \cdot \hat{2}\, \underline{r}_{12} \cdot \hat{2}\, r_{12}^{-3} \quad , \tag{A16}$$

provided, of course, that r_{12} is greater than the molecular diameter d everywhere on the surface S. (If S is ellipsoidal and $\underline{r}_1$ is inside it, recall that $J = \ell$. If S is spherical, $\underline{r}_1$ is outside it and $r_{12} > d$

on S, then $J = Q\bar{D}_{13}$, where $\underline{r}_3$ is the center of the sphere and Q is the numerical value of the volume bounded by S.) The part of (A15) independent of h_{13} is obviously $N\rho^2 \ell^2$. With the aid of (A16), the part of (A15) involving h_{13} integrates to $N\rho\, 2\pi^2/3$ from which

$$I_3 = 4N\, a^4\, E'^4\, \rho^2 (1 + \Delta^2)\, (\ell^2 + 2\pi^2/3) \quad . \tag{A17}$$

To evaluate I_4 we use (A2) to obtain

$$\Sigma_{\mu\nu\beta\gamma} \langle D^{\mu\nu}_{xx}\, D^{\beta\gamma}_{xx} \rangle = N(N-1)\,(N-2)\,(N-3) V^{-3}\, (1 - \tau/V)^{-6}$$

$$\int d^3 \underline{r}_2\, d^3 \underline{r}_2\, d^3 \underline{r}_4\, \bar{D}_{12}\, \bar{D}_{34}\, (1 - h_{13})\,(1 - h_{14})\,(1 - h_{23})\,(1 - h_{24})$$

$$= \Sigma_{i=0}^{4} K_i \quad . \tag{A18}$$

The right hand side separates naturally into terms which we call K_i where $i = 0, 1, \ldots 4$ is the number of explicit h-factors in the integrand of the term. The K_o term is integrated trivially and has a part of order N^2 which cancels the N^2 part of $\langle\langle u_2 \rangle\rangle^2$, and a part of order N, which combines with $\langle\langle u_2 \rangle\rangle^2$ from (41) (corrected by the now important factor $(1 - \tau/V)^{-1}$) to give

$$K_o - 4 \langle\langle u_2 \rangle\rangle^2 = -4 N\rho^2 \ell^2 (1 - \rho\tau) \quad . \tag{A19}$$

There are four terms in K_1 (there being four possible terms linear in one of the h's) each of which integrates trivially to $-\ell^2 \tau\rho^3$ giving

$$K_1 = -4\ell^2 \rho^3\, \tau N \quad . \tag{A20}$$

There are six ways to form integrands quadratic in the h's in (A18), four of which have one space point as an argument of both h's and are equivalent to each other. The remaining two have no space point as arguments of both h factors and are equivalent to each other. Each of the first four terms is seen to be identically zero with the aid of (A16), and the last two can be straightforwardly integrated with (A16) to give

$$K_2 = 0.5066\, \pi^2 \rho^3 \tau N \quad . \tag{A21}$$

Almost the same straightforward integrations are required for each of the four equivalent terms which are cubic in the h's and one finds that

$$K_3 = -\, 0.11713\, \pi^2 \rho^3 \tau N \quad . \tag{A22}$$

We have not been able to integrate the remaining term K_4 analytically. We estimate that it is an order of magnitude smaller than K_3 because the four h factors combine to limit the volume accessible to the points of integration much more than in K_3. Since K_3 is already a minor contribution to the final result, we feel well within the other limits of our calculation to neglect K_4 in the final result:

$$I_4 - 4 \langle\langle u_2 \rangle\rangle^2 \approx N\rho^2(-4\ell^2 + 3.84\, \rho\tau) \tag{A23}$$

combining all the above terms gives the U_{22} of (38).

BLANK PAGE

Unclassified
Security Classification

DOCUMENT CONTROL DATA - R&D
(Security classification of title, body of abstract and indexing annotation must be entered when the overall report is classified)

1 ORIGINATING ACTIVITY (Corporate author) Hughes Research Laboratories A Division of Hughes Aircraft Company Malibu, California	2a REPORT SECURITY CLASSIFICATION UNCLASSIFIED 2b GROUP N/A

3 REPORT TITLE

High Powered Diffraction Limited Raman Laser

4 DESCRIPTIVE NOTES (Type of report and inclusive dates)

Final Report, 15 May 1965 through 14 April 1966

5 AUTHOR(S) (Last name, first name, initial)

McClung, F. J., Close, D. H., Hellwarth, R. W., and Wagner, W. G.

6. REPORT DATE	7a. TOTAL NO. OF PAGES	7b. NO. OF REFS
May 1966		20

8a. CONTRACT OR GRANT NO. Nonr 4849 (00) b. PROJECT NO. Project Code No. 4730 c. ARPA Order No. 306 d.	9a. ORIGINATOR'S REPORT NUMBER(S) N/A 9b. OTHER REPORT NO(S) (Any other numbers that may be assigned this report) N/A

10. AVAILABILITY/LIMITATION NOTICES

Distribution of this document is unlimited.

11. SUPPLEMENTARY NOTES	12. SPONSORING MILITARY ACTIVITY
N/A	Department of the Navy Office of Naval Research Washington D. C. 20360

13 ABSTRACT Problems associated with the realization of a high energy, highly coherent Raman laser have been investigated. Since the discovery that the self-focusing of pump radiation and scattered radiation is present in most laboratory Raman lasers and tends to spoil the coherence of the output, the nature and mechanisms of this self-trapping have been the primary objects of study in order that it might be prevented. Time resolved photographic studies have been made which show that the small filaments of self-trapped light in the pump beam persist for only a small fraction of the beam pulse duration and are sufficiently intenst to resolve the apparent discrepancy between the average intensity and observed Raman gains. Time integrated photographic studies and photometric studies showed that only purely linearly polarized light preserves its polarization after self-trapping in CS_2 and nitrobenzene. Attempts to compare measured nonlinear indices for both circular and linear polarizations with those calculated for various mechanisms were frustrated by this instability in the propagation of circularly polarized light. The instability was explained qualitatively and indicates that electrostriction is not a dominant mechansim. A classical statistical mechanical calculation of the nonlinear index of a liquid (with no macroscopic density changes) showed that the local redistribution of molecules is generally important. This effect will cause perfectly symmetric molecules to have a significant nonlinear index. It is therefore concluded that it is very unlikely that any room temperature liquid will perform as a high energy Raman laser material without beam deterioration due to self-focusing.

DD FORM 1 JAN 64 1473

Unclassified
Security Classification

14 KEY WORDS	LINK A		LINK B		LINK C	
	ROLE	WT	ROLE	WT	ROLE	WT
Raman Scattering Giant Pulse Laser Light Trapping Nonlinear Indices of Liquids						

INSTRUCTIONS

1. ORIGINATING ACTIVITY: Enter the name and address of the contractor, subcontractor, grantee, Department of Defense activity or other organization *(corporate author)* issuing the report.

2a. REPORT SECURITY CLASSIFICATION: Enter the overall security classification of the report. Indicate whether "Restricted Data" is included. Marking is to be in accordance with appropriate security regulations.

2b. GROUP: Automatic downgrading is specified in DoD Directive 5200.10 and Armed Forces Industrial Manual. Enter the group number. Also, when applicable, show that optional markings have been used for Group 3 and Group 4 as authorized.

3. REPORT TITLE: Enter the complete report title in all capital letters. Titles in all cases should be unclassified. If a meaningful title cannot be selected without classification, show title classification in all capitals in parenthesis immediately following the title.

4. DESCRIPTIVE NOTES: If appropriate, enter the type of report, e.g., interim, progress, summary, annual, or final. Give the inclusive dates when a specific reporting period is covered.

5. AUTHOR(S): Enter the name(s) of author(s) as shown on or in the report. Enter last name, first name, middle initial. If military, show rank and branch of service. The name of the principal author is an absolute minimum requirement.

6. REPORT DATE: Enter the date of the report as day, month, year, or month, year. If more than one date appears on the report, use date of publication.

7a. TOTAL NUMBER OF PAGES: The total page count should follow normal pagination procedures, i.e., enter the number of pages containing information.

7b. NUMBER OF REFERENCES: Enter the total number of references cited in the report.

8a. CONTRACT OR GRANT NUMBER: If appropriate, enter the applicable number of the contract or grant under which the report was written.

8b, 8c, & 8d. PROJECT NUMBER: Enter the appropriate military department identification, such as project number, subproject number, system numbers, task number, etc.

9a. ORIGINATOR'S REPORT NUMBER(S): Enter the official report number by which the document will be identified and controlled by the originating activity. This number must be unique to this report.

9b. OTHER REPORT NUMBER(S): If the report has been assigned any other report numbers *(either by the originator or by the sponsor)*, also enter this number(s).

10. AVAILABILITY/LIMITATION NOTICES: Enter any limitations on further dissemination of the report, other than those imposed by security classification, using standard statements such as:

(1) "Qualified requesters may obtain copies of this report from DDC."

(2) "Foreign announcement and dissemination of this report by DDC is not authorized."

(3) "U. S. Government agencies may obtain copies of this report directly from DDC. Other qualified DDC users shall request through _____."

(4) "U. S. military agencies may obtain copies of this report directly from DDC. Other qualified users shall request through _____."

(5) "All distribution of this report is controlled. Qualified DDC users shall request through _____."

If the report has been furnished to the Office of Technical Services, Department of Commerce, for sale to the public, indicate this fact and enter the price, if known.

11. SUPPLEMENTARY NOTES: Use for additional explanatory notes.

12. SPONSORING MILITARY ACTIVITY: Enter the name of the departmental project office or laboratory sponsoring *(paying for)* the research and development. Include address.

13. ABSTRACT: Enter an abstract giving a brief and factual summary of the document indicative of the report, even though it may also appear elsewhere in the body of the technical report. If additional space is required, a continuation sheet shall be attached.

It is highly desirable that the abstract of classified reports be unclassified. Each paragraph of the abstract shall end with an indication of the military security classification of the information in the paragraph, represented as *(TS)*, *(S)*, *(C)*, or *(U)*.

There is no limitation on the length of the abstract. However, the suggested length is from 150 to 225 words.

14. KEY WORDS: Key words are technically meaningful terms or short phrases that characterize a report and may be used as index entries for cataloging the report. Key words must be selected so that no security classification is required. Identifiers, such as equipment model designation, trade name, military project code name, geographic location, may be used as key words but will be followed by an indication of technical context. The assignment of links, rules, and weights is optional.